Journal of Renewable and Sustainable Energy

RESEARCH ARTICLE | OCTOBER 11 2024

Overview of preparation for the American WAKE ExperimeNt (AWAKEN)

Special Collection: Preparatory work for the American Wake Experiment (AWAKEN)

Patrick Moriarty ; Nicola Bodini ; Stefano Letizia ; Aliza Abraham ; Tyler Ashley ; Konrad B. Bärfuss ; Rebecca J. Barthelmie ; Alan Brewer ; Peter Brugger ; Thomas Feuerle ; Ariane Frère ; Lexie Goldberger ; Julia Gottschall ; Nicholas Hamilton ; Thomas Herges; Brian Hirth ; Lin-Ya (Lilian) Hung ; Giacomo Valerio Iungo ; Hristo Ivanov ; Colleen Kaul ; Stefan Kern ; Petra Klein ; Raghavendra Krishnamurthy ; Astrid Lampert ; Julie K. Lundquist ; Victor R. Morris ; Rob Newsom ; Mikhail Pekour ; Yelena Pichugina ; Fernando Porté-Angel ; Sara C. Pryor ; Andrew Scholbrock ; John Schroeder ; Samuel Shartzer ; Eric Simley ; Lilén Vöhringer ; Sonia Wharton ; Daniel Zalkind

J. Renewable Sustainable Energy 16, 053306 (2024)
https://doi.org/10.1063/5.0141683

Journal of Renewable and Sustainable Energy PERSPECTIVE pubs.aip.org/aip/rse

Overview of preparation for the American WAKE ExperimeNt (AWAKEN)

Cite as: J. Renewable Sustainable Energy **16**, 053306 (2024); doi: 10.1063/5.0141683
Submitted: 7 January 2023 · Accepted: 9 May 2024 ·
Published Online: 11 October 2024

Patrick Moriarty,[1,a] Nicola Bodini,[1] Stefano Letizia,[1] Aliza Abraham,[1] Tyler Ashley,[2] Konrad B. Bärfuss,[3] Rebecca J. Barthelmie,[4] Alan Brewer,[5] Peter Brugger,[6] Thomas Feuerle,[3] Ariane Frère,[7] Lexie Goldberger,[8] Julia Gottschall,[9] Nicholas Hamilton,[1] Thomas Herges,[10] Brian Hirth,[11] Lin-Ya (Lilian) Hung,[9] Giacomo Valerio Iungo,[12] Hristo Ivanov,[1] Colleen Kaul,[8] Stefan Kern,[13] Petra Klein,[14] Raghavendra Krishnamurthy,[8] Astrid Lampert,[3] Julie K. Lundquist,[1,15,16] Victor R. Morris,[8] Rob Newsom,[8] Mikhail Pekour,[8] Yelena Pichugina,[5,17] Fernando Porté-Angel,[6] Sara C. Pryor,[4] Andrew Scholbrock,[1] John Schroeder,[11] Samuel Shartzer,[18] Eric Simley,[1] Lilén Vöhringer,[19] Sonia Wharton,[20] and Daniel Zalkind[1]

AFFILIATIONS

[1]National Renewable Energy Laboratory, Golden, Colorado 80401, USA
[2]ENGIE North America, Houston, Texas 77056, USA
[3]Technische Universität Braunschweig, Braunschweig, Germany
[4]Cornell University, Ithaca, New York 14850, USA
[5]NOAA Chemical Sciences Laboratory, Boulder, Colorado 80305, USA
[6]École polytechnique fédérale de Lausanne, Lausanne, Switzerland
[7]ENGIE Laborelec, Linkebeek, Belgium
[8]Pacific Northwest National Laboratory, Richmond, Washington 98109, USA
[9]Fraunhofer Institute for Wind Energy Systems IWES, Bremerhaven, Germany
[10]Sandia National Laboratories, Albuquerque, New Mexico 87123, USA
[11]Texas Tech University, Lubbock, Texas 79409, USA
[12]University of Texas at Dallas, Dallas, Texas 75080, USA
[13]GE Vernova, Munich, Germany
[14]University of Oklahoma, Norman, Oklahoma 73019, USA
[15]University of Colorado Boulder, Boulder, Colorado 80309, USA
[16]Renewable and Sustainable Energy Institute, Boulder, Colorado 80303, USA
[17]CIRES, University of Colorado, Boulder, Colorado 80309, USA
[18]GE Vernova, Greenville, South Carolina 29615, USA
[19]ForWind—University of Oldenburg, Oldenburg, Germany
[20]Lawrence Livermore National Laboratory, Livermore, California 94550, USA

Note: This article is part of the special issue Preparatory Work for the American Wake Experiment (AWAKEN).
[a]**Author to whom correspondence should be addressed:** patrick.moriarty@nrel.gov

ABSTRACT

The American WAKE ExperimeNt (AWAKEN) is a multi-institutional field campaign focused on gathering critical observations of wind farm–atmosphere interactions. These interactions are responsible for a large portion of the uncertainty in wind plant modeling tools that are used to represent wind plant performance both prior to construction and during operation and can negatively impact wind energy profitability. The AWAKEN field campaign will provide data for validation, ultimately improving modeling and lowering these uncertainties. The field campaign is designed to address seven testable hypotheses through the analysis of the observations collected by numerous instruments at 13 ground-based locations and on five wind turbines. The location of the field campaign in Northern Oklahoma was chosen to leverage existing observational facilities operated by the U.S. Department of Energy Atmospheric Radiation Measurement program in close proximity to five

operating wind plants. The vast majority of the observations from the experiment are publicly available to researchers and industry members worldwide, which the authors hope will advance the state of the science for wind plants and lead to lower cost and increased reliability of wind energy systems.

 https://doi.org/10.1063/5.0141683

I. INTRODUCTION

Wind farm–atmosphere interactions (WFAI) are among the most poorly understood phenomena when determining energy production estimates for wind power plants,[1] causing uncertainty that leads to significant financial challenges for wind energy development and financing.[2] The historical focus of WFAI has been on characterizing the intensity, expansion, meandering, and dissipation from individual wind turbine wakes. As wind turbines and wind plants continue to grow in size, and the overwhelming majority of new turbine installations occur in proximity to preexisting farms, a number of additional phenomena become important.[3,4] These include the aggregate effect of many turbine wakes, forming a wind farm wake, which responds to and interacts with the stability of the broader atmospheric boundary layer (ABL).[5] Other important WFAI, for which there are currently few data available, include upwind blockage and modifications to the heat, moisture, and momentum exchange that impact stability and boundary-layer height. Wind farm owners are also interested in turbine response to operating in partial and fully waked conditions, as well as consequences for both power production and turbine loading. These interactions impact reliability and energy production in the wind farm environment, which the wind energy community is just beginning to understand.[6] Several innovative advanced control strategies to mitigate wake effects have been proposed, although their cost-effectiveness remains unclear due to the lack of experimental data.[7]

In the wind industry, developers of predictive tools for wakes often assume these interactions are decoupled into individual phenomena for ease of model development.[8] As such, separate models exist for many WFAI phenomena including wakes,[9,10] blockage,[11–13] flow accelerations,[14,15] internal boundary layer growth,[16,17] and turbulent fluctuations.[18,19] In reality, these phenomena are highly coupled and few observations are available to fully understand and validate their mutual interactions, particularly at the scale of modern wind turbines and wind plants. Although full coupling is intrinsic to high-fidelity models of WFAI such as large-eddy simulations[20] that are becoming more commonly used, observations are still needed to validate the full range of wind plant models.

The need for more observations to enable better understanding of WFAI inspired the U.S. Department of Energy (DOE) to fund a national laboratory-led multi-institutional field campaign called the American WAKE ExperimeNt (AWAKEN). Project planning began in March 2018 and is summarized in the overview papers of Moriarty *et al.*[21] and Debnath *et al.*[22] The deployment of instrumentation began in September 2022. This paper provides the final details of the design and observational strategy for the AWAKEN experiment, contextualized within the project's science goals, as well as examples of data produced in the experiment that we hope will benefit the wind energy and atmospheric science communities.

The AWAKEN project builds on previous field observation campaigns dating back three decades to better understand WFAI.[23] Until the early 2010s, researchers and wind farm owners primarily focused on wakes generated under flow aligned with wind turbine rows, which result in the greatest losses in energy production. One of the earliest wake studies of turbines was a series of observations[24,25] in the Netherlands, with turbines only 30 m in diameter; small by modern turbine standards and missing some important physics of larger turbines. Subsequent studies with larger turbines relied exclusively on turbine Supervisory Control and Data Acquisition (SCADA) to infer changes in wind speed within wind plants for different inflow wind directions.[26–32] In these studies, researchers estimated the wake velocity deficit at different downstream locations using power losses at each turbine. Several of these studies have been used for model validation under the International Energy Agency (IEA) Wind Technology Collaboration Program (TCP) Task 31 effort[33] and are the foundation on which many industry models are validated.[8] Later studies[28,34] from this era began to highlight the importance of atmospheric stability to wake propagation, emphasizing a weakness in models that had largely assumed the atmosphere to have near-neutral stability and neglected thermal effects on turbulence generation and dissipation. In the next generation of wind turbine wake observations, researchers deployed remote sensing devices such as sodars, radars, and lidars in the vicinity of standalone turbines and those within wind farms to more directly observe wake behavior.[35–42] Even more recently, offshore wind farms have provided greater opportunities for WFAI measurements using satellite observations,[43] aircraft,[44–47] and X-band radars.[48]

The current generation of atmospheric measurements, such as those from the AWAKEN campaign or the upcoming German WiValdi studies,[49] are leveraging the experiences of previous campaigns by using similar types of remote sensing instrumentation, but in greater number and with longer range and higher fidelity. There is also greater emphasis on gaining more detailed observations of individual turbine response. One unique aspect of the AWAKEN project is the incorporation of wind farm control studies that aim to modify turbine operations to influence the WFAI (primarily wakes) such that the overall energy production of the wind farm is improved with acceptable impact on turbine reliability.[6]

In this paper, we begin with a summary of the testable hypotheses for the AWAKEN project in Sec. II, which provides context for the choice of the project site, as explained in Sec. III. We then walk through each hypothesis in Sec. IV to explain the placement and observational strategies of instruments gathering the measurement data needed to achieve the science goals of the project. Finally, we describe our data management approach in Sec. V, and we present conclusions in Sec. VI.

II. TESTABLE HYPOTHESES

By both observing and simulating the atmospheric boundary layer in the region within and around operational wind farms, the

AWAKEN project aims to address several testable hypotheses, which were identified and prioritized at a technical experts meeting in 2018 (Ref. 21) and are listed here in order of priority, the highest priority being listed first:

(1) Wind farm wakes propagate on land for tens of kilometers and lower the energy production of neighboring wind farms. Characteristics (magnitude and extent of momentum deficits, magnitude and extent of the region of increased turbulence kinetic energy [TKE]) of wind plant wakes depend primarily on the spacing of turbines in a wind farm along the primary wind direction, turbine size, individual turbine power level and hub-height TKE (or turbulence intensity), wind speed at hub height, and atmospheric stability. Wind farm wakes can be steered using coordinated individual turbine yaw control, although topography and yaw-misalignment will also influence wake propagation.
(2) Wind turbines in the interior of land-based wind farms tend to have more turbulent inflows resulting in higher damage-equivalent loads than those on the exterior. The turbulence levels in land-based wind farms asymptote to a fully developed condition after the first three rows of wind turbines.
(3) The decrease in hub-height flow wind speed 1–30 rotor diameters (D) upwind of a land-based wind farm due to wind farm blockage, which changes power production and increases prediction uncertainty, depends on turbine operation, atmospheric stability, inflow wind speed, boundary-layer height, wind shear, and veer (interacting with wind turbine characteristics, wind farm layout, terrain and surface roughness, and operative condition). Furthermore, the blockage may create wind speed-up along the edges of the wind farm.
(4) Wake steering and turbine consensus control increase full wind farm power production and reduce structural loads of turbines under a specific range of atmospheric conditions. The overall benefit of wind farm control is primarily dependent upon inflow winds, atmospheric stability, boundary layer height, wind shear and veer, and wind direction variability (interacting with the turbine type, orography, inter-turbine spacing, and alignment), with maximum benefit coming when columns of turbines are aligned with wind direction under stable conditions.
(5) The maximum energy produced by a large (>100 MW) land-based wind farm is constrained by the momentum flux between the surrounding atmosphere and the flow within the wind farm.
(6) Individual turbine wake morphology, evolution, and wake interactions are affected by a complex interplay of events connected to turbine settings, control, and short-term variability of the incoming wind conditions. Including a stochastic component to wake, turbulence, and turbine models will enable higher accuracy for predictions of wind turbine wakes and their interactions.
(7) Intermittent atmospheric turbulent bursting events related to Kelvin–Helmholtz instability, gravity waves, and bores lead to fluctuations in wind farm power production and structural loading of wind turbines.

III. PROJECT LOCATION

The AWAKEN field campaign takes place in northern Oklahoma (Fig. 1) approximately 100 km north of Oklahoma City. A primary driver for selecting this location is its proximity to the DOE Atmospheric Radiation Measurement (ARM) Program's Southern Great Plains (SGP) facility, a suite of atmospheric measurement sites that have been in continuous operation since 1992.[50,51] The SGP is the world's largest climate field supersite with over 55 000 acres and more than 30 instrument clusters centered 42 km northeast of Enid, Oklahoma. Some of these instrumented sites are shown in Fig. 1.

Not only does this site offer a unique array of historical and ongoing atmospheric measurements, but it is also located in a wind resource-rich area with numerous surrounding wind power plants. There are five wind plants in the AWAKEN field campaign area, all south of the ARM SGP central facility (denoted as C1 in Fig. 1): Chisholm View, Thunder Ranch, Breckinridge, King Plains, and Armadillo Flats. Some details of each are highlighted in Table I, including year of first operation, total rated power, total number of wind turbines, turbine models with rotor rated power and diameter, and farm net capacity factor. The total installed capacity is nearly 1.19 GW of power generated by 558 turbines. Capacity factors are determined as the ratio of actual power generation to the maximum power production if each turbine were operating at its rated capacity for one year. The reported net capacity factors are calculated as an average from the annual net generation values reported by the U.S. Energy Information Administration (EIA).[52] For each wind plant, data for the first year reported by the EIA are not considered in the calculation. The hub heights of the turbines in the Thunder Ranch, King Plains, and the 2.3 MW turbines in Armadillo Flats are 89 m, while the remaining turbines have hub heights of 80 m. For the AWAKEN project, the King Plains wind plant was chosen for a detailed study, as it is the newest wind plant in the area with the largest turbines, which have the most modern control systems for easier implementation of wind plant control studies.

One scientific topic of interest related to the first testable hypotheses on wind farm wakes is the impact that the nearby wind farms have on the observations from the ARM instrumentation. Since its inception, the ARM SGP observations have been used by the world's meteorological and climate modelers. As wind farms have been installed in the area, the research community has expressed interest in quantifying the extent to which these observations are biased by the wind plants, which have been built around the measurement sites.

Krishnamurthy *et al.*[54] offers a detailed analysis of the atmospheric conditions in the area using the long-term observations collected at ARM SGP. The dominant wind direction in the area is southerly (Fig. 2),[22,54] meaning wind plants to the south are most likely to impact ARM SGP measurements throughout a given year.

Wharton *et al.*[55] completed one of the earliest studies that examined wind flow characteristics specifically at rotor-disk height at the ARM SGP facility. At that time, the facility was neighbored by only a single wind farm (Chisholm View) to the west, a wind direction not commonly seen at the ARM site, and thus the impacts were found to be negligible. In recent years, wind farms have been built upwind of the SGP, making WFAI both more relevant and complex to observe and quantify. Bodini *et al.*[56] quantified the long-term impact of the newer wind plants on long-term observations of surface winds, winds aloft, and TKE at the ARM SGP, using both ARM observations and mesoscale simulations incorporating a wind farm parameterization. They found some impacts were appreciable, such as a 30% increase in TKE under stable conditions, reinforcing the need to gather more

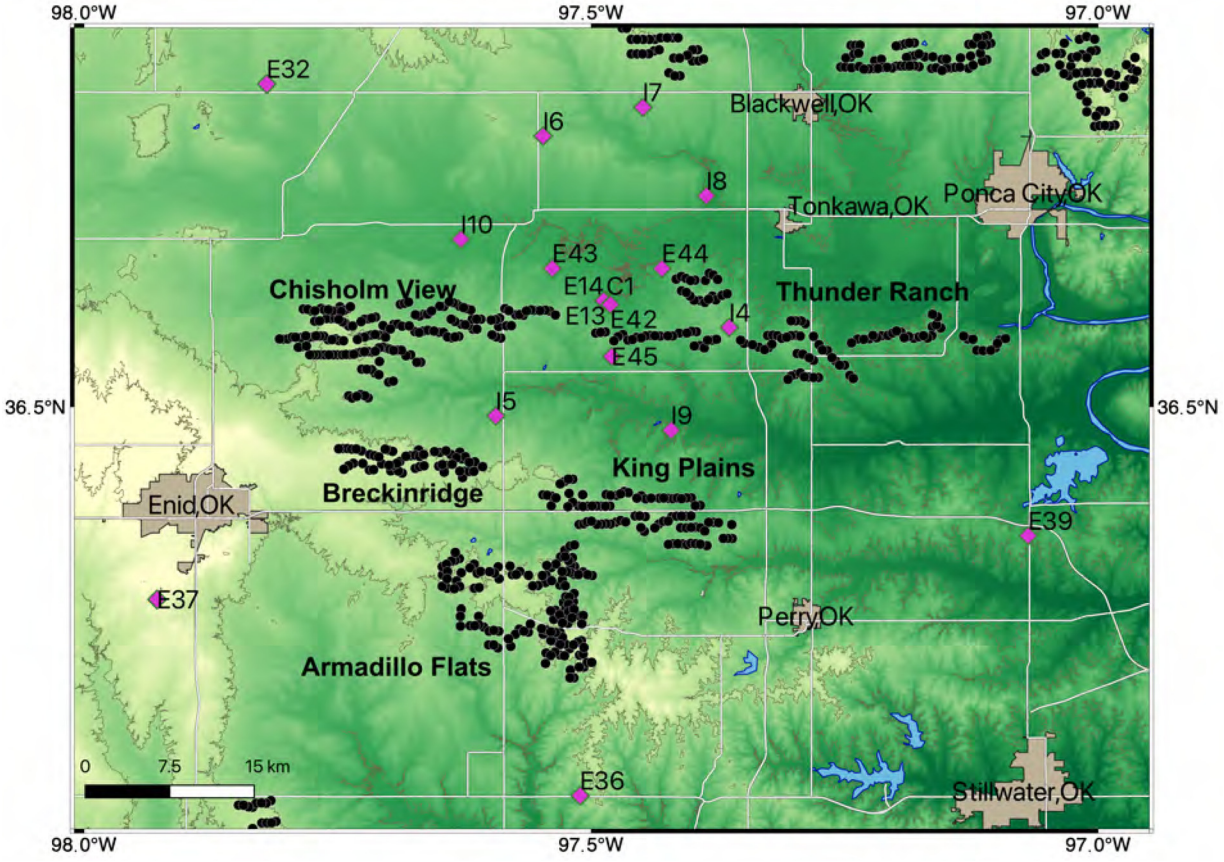

FIG. 1. DOE ARM instrument cluster field sites (labeled as magenta diamonds) within Northern Oklahoma and surrounding wind plants (black dots). The white lines are roads, and brown areas depict towns.

TABLE I. Wind plants within the AWAKEN project area. The specific locations of the wind turbines can be found in the U.S. Wind Turbine Database.[53]

Wind farm	Operational since	Total power	No. of turbines	No. of each turbine model (rotor diameter)	Net capacity factor
Chisholm View	2012	300 MW	167	140 × GE 1.68 MW (82.5 m) 27 × GE 2.4 MW (107 m)	0.35
Thunder Ranch	2017	297.8 MW	120	109 × GE 2.5 MW (116 m) 11 × GE 2.3 MW (116 m)	0.41
Breckinridge	2015	96.9 MW	57	GE 1.7 MW (103 m)	0.49
Armadillo Flats	2018	241.8 MW	126	80 × GE 1.7 MW (103 m) 46 × GE 2.3 MW (116 m)	0.43
King Plains	2020	248.2 MW	88	GE 2.82 MW (127 m)	0.37

observations to help quantify the impact not only for the wind energy community but also for all the atmospheric scientists who routinely analyze SGP observations.

IV. INSTRUMENTATION PLACEMENT

Instruments were placed within the AWAKEN field domain based on the prioritized set of testable hypotheses. The majority of instruments are deployed in and around the King Plains Wind Farm. Data from the existing 90-m meteorological tower at this wind farm are also available to AWAKEN researchers. There are a total of 13 ground-based field sites in the campaign hosting a variety of instruments in addition to instruments placed on five instrumented King Plains wind turbines (Fig. 3). The site locations were selected such that the instruments can provide observations at adequate spatial resolution to address the project science goals. Table II provides an overview of the deployed instrumentation at each site, their primary flow region of

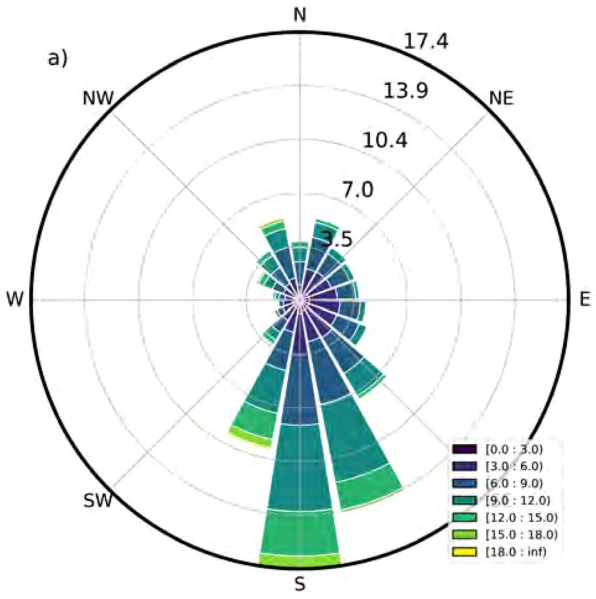

FIG. 2. Wind rose from three years of observations from the King Plains wind plant meteorological tower (28 km SSE of ARM central facility) measured at 91 m above ground level (AGL). Reproduced with permission from Debnath *et al.*, J. Phys.: Conf. Ser. **2265**, 022058 (2022), IOP Publishing.[22]

observation, and their associated testable hypotheses. We note that not all the instruments listed in Table II remained deployed for the whole duration of the field campaign. For more detailed information on the precise location and deployment timeline of each instrument, users should refer to the data portal, described in Sec. V.

In addition to the permanent instrumented sites listed in Table II, observations during AWAKEN were also taken using mobile devices, which were deployed at AWAKEN over shorter periods of time: a truck-mounted lidar and a research aircraft, both primarily focused on characterizing wind farm wakes.

The turbines themselves also provide information of their operational state through each turbine's SCADA system, which is useful for all testable hypotheses. SCADA data include power output, wind speed, and direction as measured by turbine mounted sensors, which can be used to infer the flow in between turbines in the wind farm. Other channels are useful for inferring the turbine response, which applies to testable hypotheses 2 and 4. SCADA data are available to researchers (who are part of a nondisclosure agreement with the wind plant owners and turbine manufacturer) for all turbines within the five operational wind farms of Table I at a minimum temporal resolution of 10 min, with many channels available at higher frequencies of up to 0.5 Hz depending on the turbine and data channel.

A. Inflow

Observations of the inflow conditions into the wind plants are essential for all the testable hypotheses, which depend on an accurate

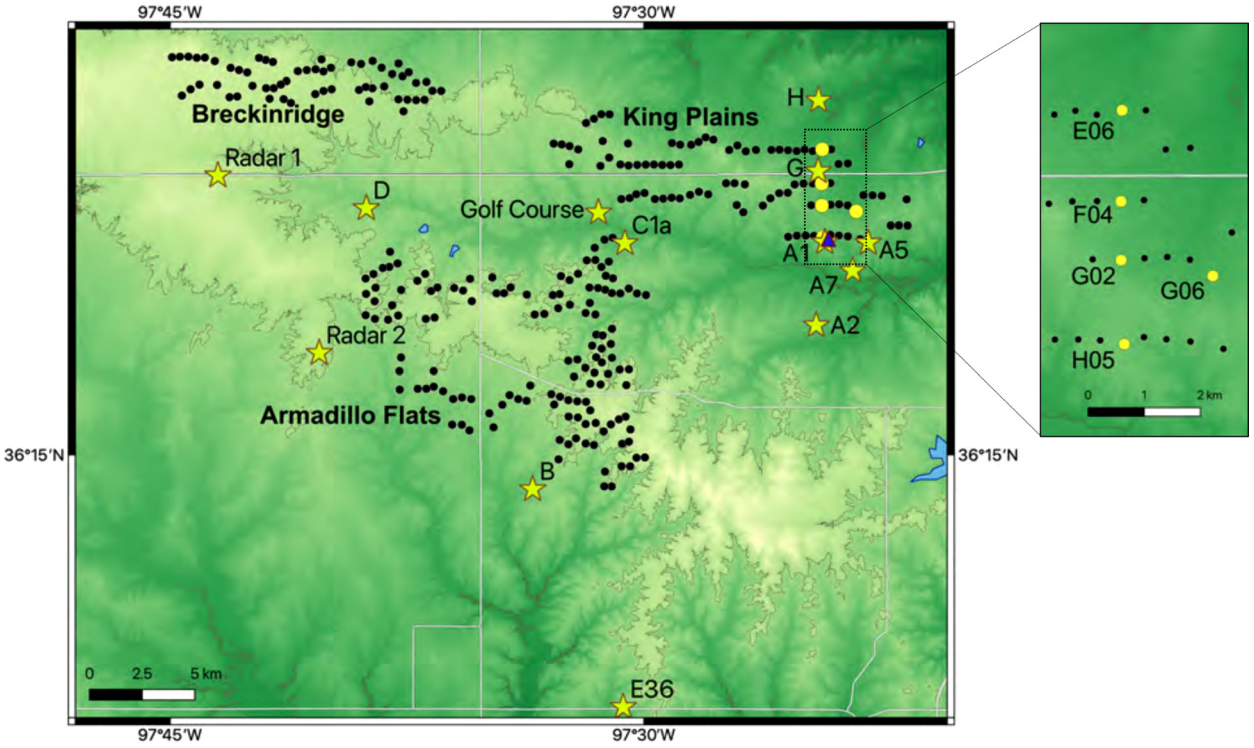

FIG. 3. Map of the field sites where AWAKEN instruments were deployed (yellow stars), the existing King Plains meteorological tower (blue triangle), and a zoomed-in map showing the five instrumented turbines (yellow dots).

TABLE II. List of instrumentation deployed as part of the AWAKEN field campaign. Legend: SL = scanning lidar, PL = profiling or fixed-beam lidar, TP = thermodynamic profiler, FS = surface flux station, MS = meteorological station, C = ceilometer, MR = microwave radiometer, R = radiation measurement, P = precipitation sensor, X = X-band radar, TS = tethersonde, RS = radiosonde, L = load measurement. The testable hypotheses are identified by the item number in the list provided in Sec. II.

Site	Flow region	Testable hypothesis	SL	PL	TP	FS	MS	C	MR	R	P	X	TS	RS	L
A1	Inflow	2, 3, 5, 7	✓	✓	✓	✓	✓	✓		✓	✓		✓		
A2	Inflow	3, 5, 7	✓	✓		✓	✓								
A5	Inflow	2, 3	✓	✓		✓	✓								
A7	Inflow	3	✓				✓								
B	Inflow	5, 7		✓	✓		✓								
C1a	Inter-farm	1, 5, 7	✓	✓	✓	✓	✓								
D	Inter-farm	1		✓											
E36	Inflow	5, 7	✓	✓	✓				✓						
G	Intra-farm	2			✓	✓	✓						✓		
Golf Course	Inter-farm	1, 5, 7	✓	✓	✓				✓						
H	Downwind	1, 5, 7	✓	✓	✓	✓	✓	✓	✓	✓	✓			✓	
Radar 1	All	1, 3, 6	✓									✓			
Radar 2	All	1, 3, 6										✓			
Turbine H05	Inflow	2, 3, 4, 6, 7	✓	✓							✓				✓
Turbine G02	Intra-farm	2, 4, 6, 7	✓												✓
Turbine F04	Intra-farm	2, 4, 6	✓												
Turbine E06	Downwind	1, 2, 4, 6, 7	✓												✓
Turbine G06	Intra-farm	3, 4, 6	✓												

characterization of the profiles of incoming wind speed, wind direction, turbulence, temperature, and moisture. The primary ground sites for inflow characterization at AWAKEN, assuming predominantly southerly flow, includes the following: site B, just south of Armadillo Flats; site E36, even further south; sites A1, A2, A5, and A7, all south of King Plains; and the existing King Plains meteorological tower.

Sites A1, A2, A5, B, and E36 all include a profiling lidar, which provides vertical profiles of flow statistics (wind speed, direction, and turbulence intensity) in the lowest ∼200 m. AWAKEN uses two primary types of profiling lidars: pulsed lidars (WindCube v1, v2, and v2.1) and continuous wave lidars (ZephIR300 and ZX300). TKE is derived from the high-frequency u, v, and w wind components to quantify the magnitude of 3D turbulence. Note that the pulsed lidars output data at a slightly higher frequency than the continuous wave for the entire measurement profile. This is because it takes approximately 15 s to complete a scan with the continuous wave lidars and 4 s with a pulsed lidar. A second difference between the two types is the probe depth or range gate, which is a constant 20 m in the pulsed lidars but differs with measurement height (e.g., 1.4 m at 10 m up to 15.4 m at 100 m) for the continuous wave lidars. Even so, these instrument differences should not result in large measurement differences for energy scales at low wave numbers ($k < 0.005$ m^{-1}).[57] One possible drawback of these instruments is their reliance upon the assumption of horizontal statistical homogeneity of the flow, which is expected to break down if wakes or turbine induction effects are present within the scanning volume. Moreover, the direct approach to estimate TKE from the profiling lidars is the possible overestimation of variances due to the cross-contamination.[58] The impact of these effects is strongly dependent on the statistical properties of the flow and hence is site- and time-dependent, which makes an *a priori* error quantification highly uncertain.

Sites A1 and A2 also include scanning lidars, which are used in both vertical profiling and vertical stare mode, and effectively vertically extend the observations of the co-located profiling lidars up to a few kilometers. These lidars provide additional flexibility in the programming of the scan geometry, which can be leveraged to mitigate some of the undesired effects that impact profiling lidars. The scanning strategy adopted for wind profiling is the six-beam scan developed by Sathe *et al.*[59] This scan allows retrieval of not only first-order wind statistics but also the full Reynolds stress tensor through a linear transformation of the variance of the line-of-sight wind speed.[60] This type of scan assumes horizontal statistical homogeneity of the flow, but it is theoretically devoid of the cross-contamination effect that corrupts second-order statistics obtained by applying the eddy covariance method of a profiling lidar.

Given the proximity of site A1 to the southernmost row of King Plains wind turbines (∼ 2.5D), which could lead to a violation of the horizontal flow homogeneity assumption, the scanning strategy of the lidar at A1 has been properly adapted. The six-beam scan has been re-optimized by introducing a constraint that prevents the beams from probing the region to the north of site A1, where the induction of the turbines may create spatial gradients, especially of mean wind speed. The novel "tilted" six-beam scanning strategy was validated prior to the campaign by comparing the lidar retrieval to the turbulent statistics obtained from the sonic anemometers installed at 119 m on the M5 met tower at the National Wind Technology Center.[61] One of the scanning lidars of the AWAKEN fleet was installed in proximity to the M5 met tower and performed alternatively regular and tilted six-beam scans for a duration of 10 min for 3 months in spring/summer 2022. Figure 4 shows a comparison of key wind statistics (wind speed, direction, TKE, and turbulent shear stress) between the lidar performing the regular six-beam and the tilted one (top and bottom panels,

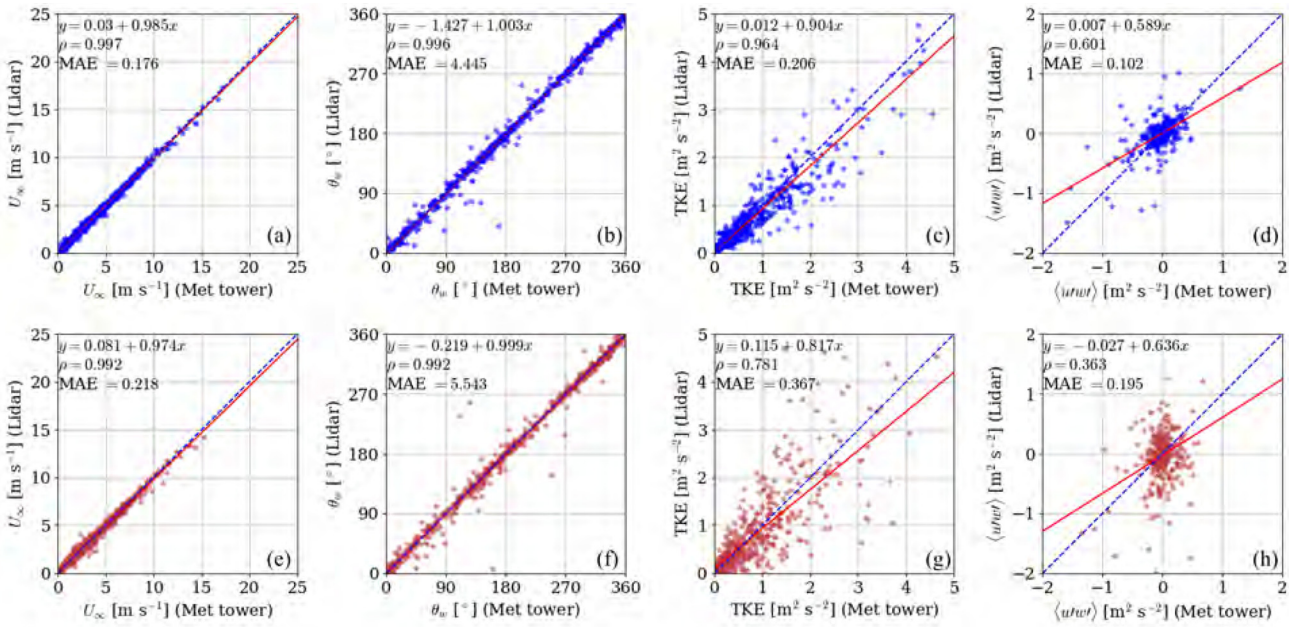

FIG. 4. Comparison between wind statistics at 119 m AGL from the met tower and the scanning lidar performing 6-beam profiling in the conventional configuration (a)–(d) and inclined one (e)–(h). (a) and (e) wind speed; (b) and (f) wind direction; (c) and (g) TKE; (d) and (h) vertical turbulent stress. The linear fit parameters, correlation coefficient (ρ), and mean absolute error (MAE) are also prompted as error metrics.

respectively). The accuracy in the reconstruction of mean quantities is unaffected by the scanning mode, with a goodness of fit comparable to that of the original publication.[59] The second-order statistics, instead, are mildly affected by scan geometry with correlation coefficients that drop from $\rho = 0.964$ to $\rho = 0.781$ and $\rho = 0.601$ to $\rho = 0.363$ for TKE and shear stress, respectively. However, the lower but quantifiable fidelity of the tilted scan in reproducing wind statistics has been deemed acceptable given the unknown effect that turbine induction could cause to a regular scan. The quantification of the wind plant induction is indeed one of the scopes of AWAKEN, and it is not known *a priori*. Figure 5 shows an example of vertical profiles from site A1 during a typical clear-sky day during the AWAKEN campaign. Interesting features are the evident nocturnal low-level jet lasting through the early morning (03:00–15:00 UTC, where UTC is the local time +5 h) and the drastic increase in TKE during the daytime, a clear signature of the development of a vigorous convective boundary layer.

Inflow sites A1 and B also host infrared spectrometers (IRSs), which are used as thermodynamic profilers to characterize the vertical profile of temperature and humidity upwind of the wind plants. The IRS at site B, as well as those at sites C1_a and G, run the latest version of the Tropospheric Remotely Observed Profiling via Optimal Estimation (TROPoe) algorithm.[62] The accuracy of the retrieval has been assessed during a pre-campaign deployment at NREL's National Wind Technology Center where several days of TROPoe retrievals have been compared to the observation provided by the previously mentioned M5 met tower. Figure 6 shows the time series of observed temperature and mixing ratio from TROPoe superposed to their met-tower equivalents. In spite of the profoundly different measuring principles between the IRS+TROPoe system and the met tower, the agreement for temperature [Fig. 6(a)] is excellent ($\rho = 0.993$, and MAE $= 0.62\,^{\circ}$C). The mixing ratio [Fig. 6(b)] also shows a fair agreement ($\rho = 0.896$, MAE $= 0.53\,\mathrm{g\,kg^{-1}}$), although the two signals are significantly different during periods of precipitation (blue band on top of the figure). This discrepancy is likely due to wet met tower sensors and is not particularly concerning. Figure 7 shows the thermodynamic profiles at site B during a clear-sky day. The temperature profiles [Fig. 7(a)] exhibit the expected diurnal cycle with the development of a thin stable ABL at nighttime and a sharp reversal of the lapse rate after sunrise. Moisture [Fig. 7(b)] appears to be confined close to the surface in night compared to daytime. It is noteworthy that the IRS+TROPoe system is also capable of detecting a capping inversion around 500–750 m, which is valuable information for mesoscale simulations aiming at capturing ABL–wind plant interactions.

For portions of the AWAKEN campaign, the Collaborative Lower Atmospheric Mobile Profiling System (CLAMPS)[63] is deployed at the ARM-owned E36 site. The CLAMPS unit includes a scanning lidar, thermodynamic profiling system, and microwave radiometer, and thus represents an additional important source of inflow conditions further south in the AWAKEN domain.

Surface inflow conditions are also important since they provide the bottom boundary conditions for numerical simulations and important scaling and stability parameters for the analysis of atmospheric and turbine data. High-frequency surface measurements and the associated turbulent fluxes are available at sites A1, A2, and A5, whereas 1-Hz wind speed, direction, temperature, pressure, and relative humidity are measured by the surface stations at sites A1, A2, A5, A7, and B. The King Plains meteorological tower complements these inflow measurements of wind speed by providing high-resolution turbulence statistics.

Dual-Doppler lidar techniques are also employed to characterize the inflow. The scanning lidars at sites A5 and A7 are coordinated to

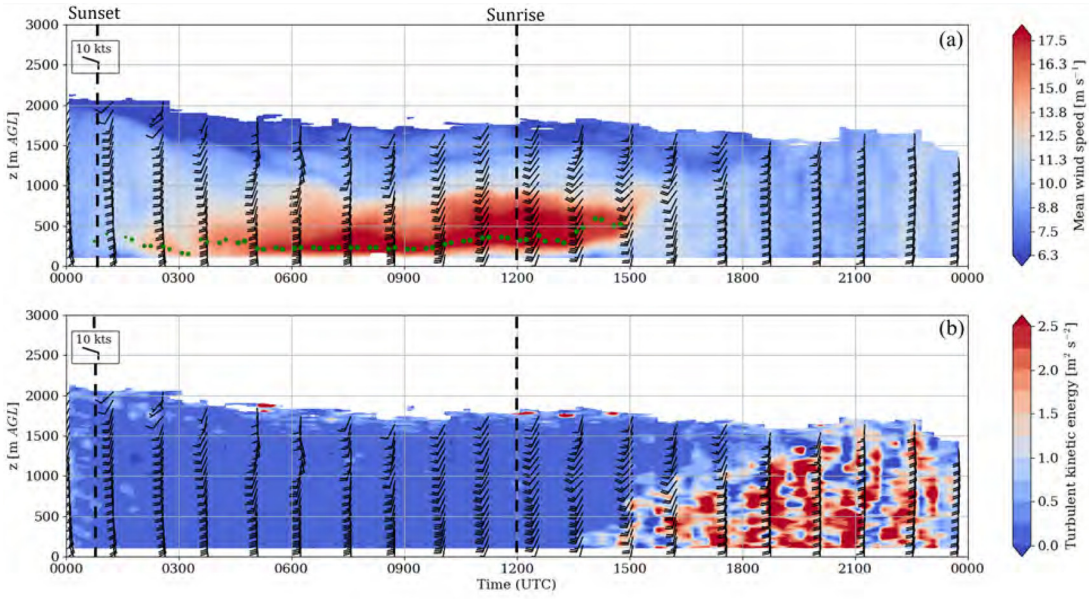

FIG. 5. Inflow reconstructed from the scanning lidar at site A1 on April 12, 2023. (a) Mean wind speed, where the location and magnitude of the green dots indicate the nose height and class of the low-level jet, respectively; (b) TKE.

create a linear array of virtual towers[64,65] at varying distances south of the leading row of turbines in the King Plains Wind Farm. Section IV D provides additional details on the scanning strategy adopted by these two lidars, which is particularly useful for investigating blockage.

Finally, additional inflow measurements are provided by the nacelle-mounted lidars on turbine H05. The turbine has a scanning lidar to probe the inflow in a wide region, and a Windcube nacelle lidar that provides a higher-resolution characterization of the inflow along the turbine horizontal axis in terms of wind speed, inflow direction, shear, and turbulence intensity.

B. Wind farm wakes

The understanding of wind farm wakes is the highest priority testable hypothesis for the AWAKEN project. Observed offshore

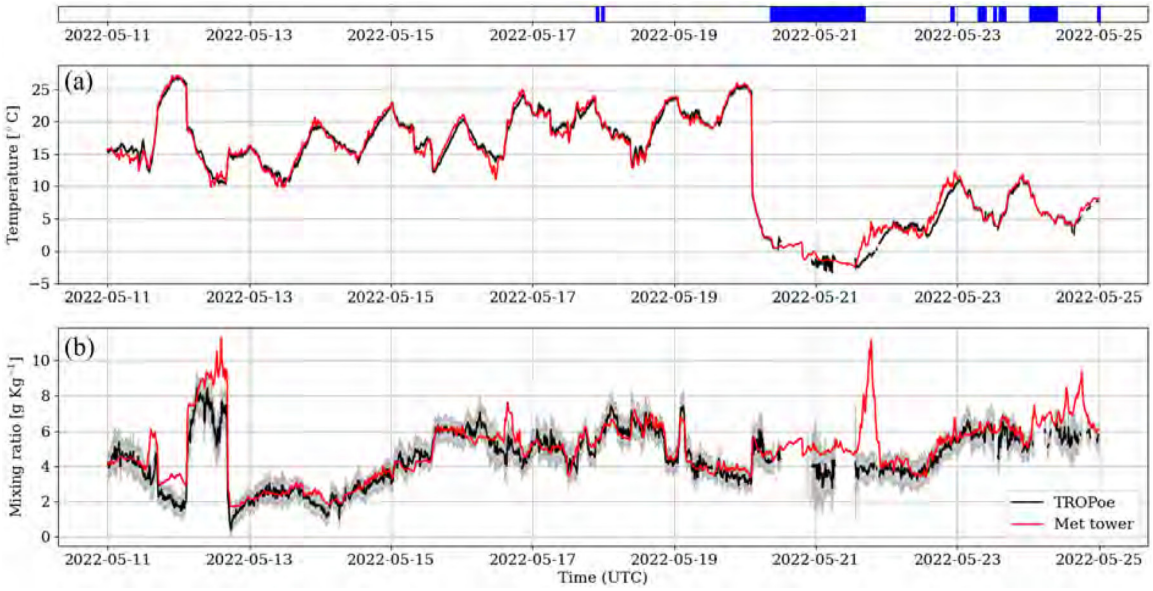

FIG. 6. Comparison of temperature (a) and mixing ratio (b) obtained by TROPoe and the observation of M5 met tower at 87 m AGL. The shaded area represents the 95% confidence interval of TROPoe. The blue bands at the top correspond to periods when precipitation was detected at the ground.

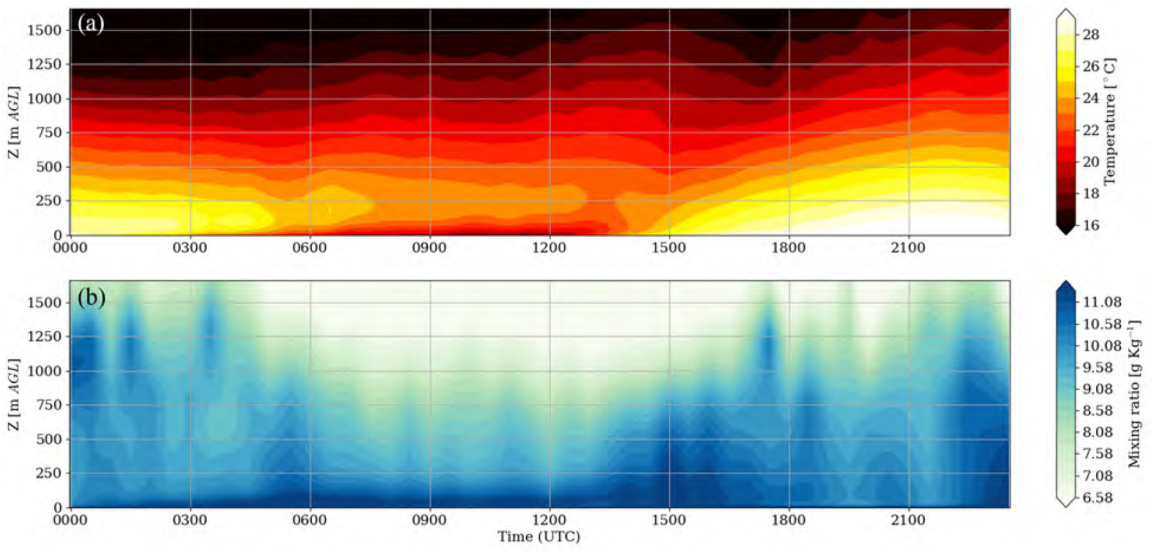

FIG. 7. Temperature (a) and mixing ratio (b) profiles retrieved through TROPoe at site B on June 6, 2023.

wakes have extended up to 50 km downwind,[66] and simulated wakes have extended even further.[5,56,67–69] This large spatial extent means that instruments must be placed further apart in the field campaign domain and have longer range than those observing individual turbine wakes.

One unique set of instruments to observe wind farm wakes are custom X-band radar systems developed at Texas Tech University.[70] Similar instruments have been deployed for a commercial offshore project in the Ørsted Beacon project,[48] and AWAKEN represents their first deployment in a dual-Doppler configuration for an onshore wind farm wake experiment. For the AWAKEN configuration, the radars implement a maximum range of 35 km and horizontal data resolution of 0.5° in the azimuthal dimension and 9 m in the along-beam dimension. The deployment locations were chosen to most effectively provide overlapping data coverage from both radars in the area between Armadillo Flats, Breckinridge, and King Plains (Fig. 8), allowing for dual-Doppler wind field reconstruction in this region. The scanning strategies implemented by these radars have been optimized to document the horizontal extent of the wind farm and individual turbine wakes. Although considerable terrain change occurs throughout the

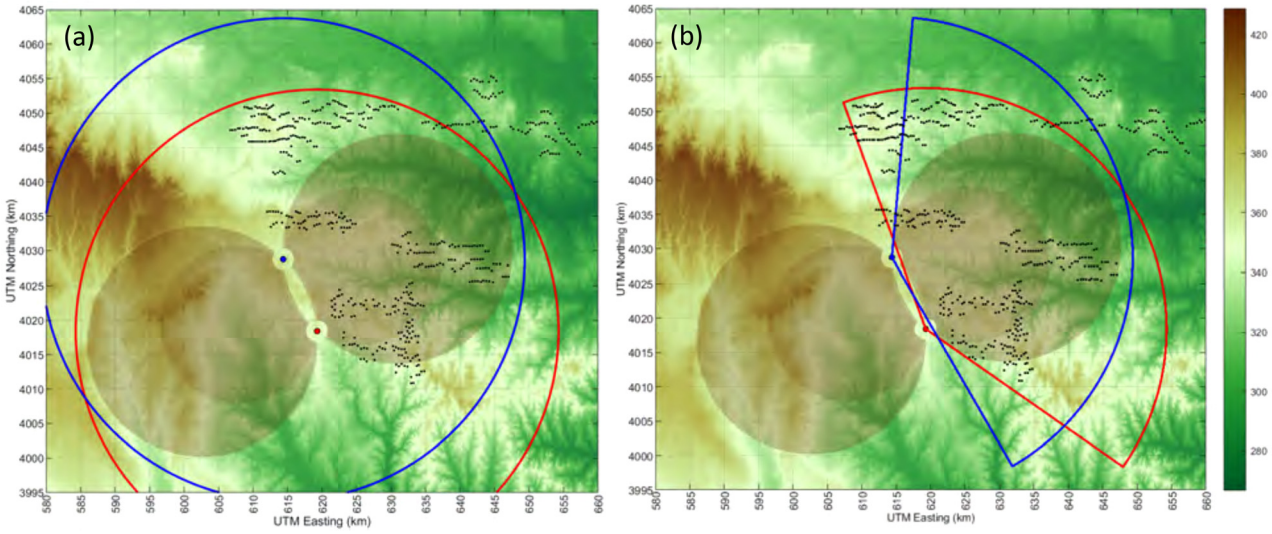

FIG. 8. Maps showing the deployment location of the two X-band radars at AWAKEN, and (a) their 360° surveillance coverage and (b) the sectors they scan at AWAKEN to allow for the dual-Doppler retrievals. Underlying contours show terrain elevation in m ASL.

broad radar coverage area, focus has been placed on collecting measurements through the depth of the rotor sweep of as many turbines within the domain as possible. For example, there exists a 120 m elevation difference between the north radar and the easternmost turbine in King Plains located at a range of roughly 32 km; 40 m due to terrain change and 80 m due to the Earth's curvature. A long-range scanning lidar at Radar site 1 and a profiling lidar at site D (see Fig. 3) are used to verify, potentially calibrate, and supplement the radar measurements.

Figure 9 shows an example velocity field obtained by the radars under stable nighttime conditions. With wind from the east, the wake of the King Plains wind plant is seen propagating to the west, reaching the edge of the radar domain, and impinging on the northern portion of Armadillo Flats. Effects of plant layout are also visible, with bands of low- and high-speed flow indicating wakes of turbine rows and gaps between rows, respectively.

Because of the dominance of southerly flow in the area, appropriate sites to quantify the extent of wind farm wakes are north of the wind farms: sites C1_a, the Golf Course, and site H. At each of these sites, scanning lidars with ranges of up to 5 km measure both the horizontal and vertical extent of the wind farm wakes downwind of Armadillo Flats (at C1_a and the Golf Course) and King Plains (at H). All the lidars at the three mentioned locations carry out wind profiling, while the instruments at C1_a include volumetric scans aimed at probing the intra-farm region in a 3D fashion.[71] Additionally, the observations collected by the nacelle-mounted scanning lidar on turbine E06 (see Sec. IV G for details on the scanning strategy), as well as those collected by NOAA's truck-mounted scanning lidar and the Technische Universität Braunschweig's research aircraft are essential in documenting the variability of wind farm wakes.

In the past, analyses of wind farm wakes have primarily focused on the variability of the velocity field. More recently, observations have also shown wind farm impacts on near-surface temperature and humidity[72–76] and higher up with aircraft measurements.[66] For the

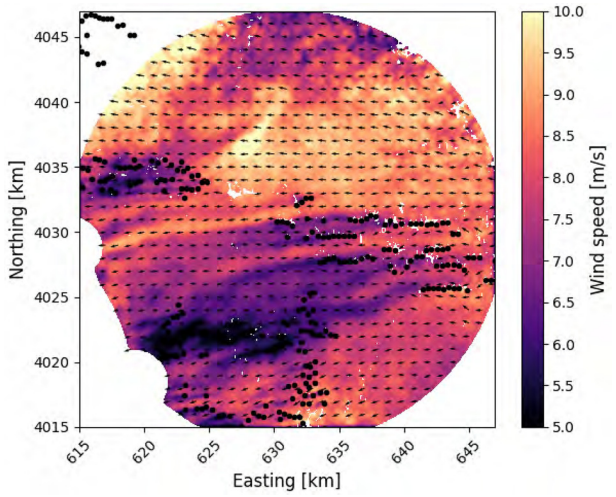

FIG. 9. Velocity field at 450 m elevation ASL captured by the dual-Doppler X-band radars on June 15, 2023 at 05:05:50 UTC, with wind from the east. Vectors indicating wind velocity magnitude and direction are shown every 20 grid points for visibility.

AWAKEN project, researchers are observing full vertical profiles of temperature and humidity downwind of wind plants using the thermodynamic profiling systems deployed at sites C1_a, G, and H, providing one of the first-ever insights into the effect of farm wakes on the microclimate across the ABL height.

The mobile instruments deployed at AWAKEN are also used to further characterize wind farm wakes north of King Plains.

A truck-mounted motion-compensated micropulsed lidar called PUMAS (PickUp-based Mobile Atmospheric Sounder) operated by the National Oceanic and Atmospheric Administration (NOAA) was used to collect observations of wind speed in the wake of the King Plains wind plant from August 15 to September 15, 2023. The Micropulsed Doppler (MD) lidar is a compact system designed for operations from mobile platforms such as aircrafts, ships, and ground vehicles. The MD lidar measurements include a vertical stare and scanning capability to provide the three components of wind velocity profiles from 46 m up to 4 km AGL with a vertical resolution of 25 m and a spatial resolution of 750 m along the driving path. Pointing errors during vertical stares were reduced by the use of a motion stabilization platform to compensate for platform motion. The accuracy of measurements from PUMAS was tested against the measurements from stationary scanning lidars during several experiments prior to AWAKEN. The results show that the pointing stabilization precision of vertical velocity is less than 0.06° RMS (root mean square), and the pointing accuracy is about 0.15°. Calculated and removed platform motions allowed the acquisition of vertical velocity with 1–2° RMS in pitch, roll, and with ± 1–2 m s^{-1} vertical error due to the heave motions. The optimized driving pattern around and within the King Plains wind plant is illustrated in Fig. 10.

The research twin propeller aircraft Reims-Cessna F406 operated by the Technische Universität Braunschweig was flown at low altitude north of King Plains in late August and September of 2023. The instrumentation on board consists of different sensors to measure wind vectors, temperature, and humidity at high temporal resolution. In addition, surface properties (surface temperature and geometric surface roughness) are measured, and the radiation budget is quantified with both nadir and zenith hemispheric sensors for solar and terrestrial irradiance. Based on the experience of pronounced offshore wakes for stable atmospheric conditions,[46] and previous simulations of wake propagation from onshore wind farms,[3] the flights were conducted in the early morning, between sunrise and the onset of turbulent mixing, when stable conditions can be expected. The flight pattern for the predominant wind direction from south consisted of several W–E legs at hub height north of the King Plains wind plant at different distances from the northernmost turbines (500 m, 2 km, 5 km, and 10 km), see Fig. 11(a). Due to the sloping terrain, a change in altitude was taken into account in the flight trajectory [Fig. 11(b)] to preserve the measurement height with respect to the ground, as the flow is likely to be terrain-following at low altitudes. In addition, vertical profiles between the surface and altitude of 1 km were performed at the eastern edge of the flight legs to probe the temporal development of atmospheric stability and the wind profile.

C. Interior turbulence and turbine response

The evolution of turbulent structures, statistics, and dissipation rates within wind farms has been explored with some detail through numerical simulation,[77–80] laboratory-scale wind tunnel experiments,[81–84] and

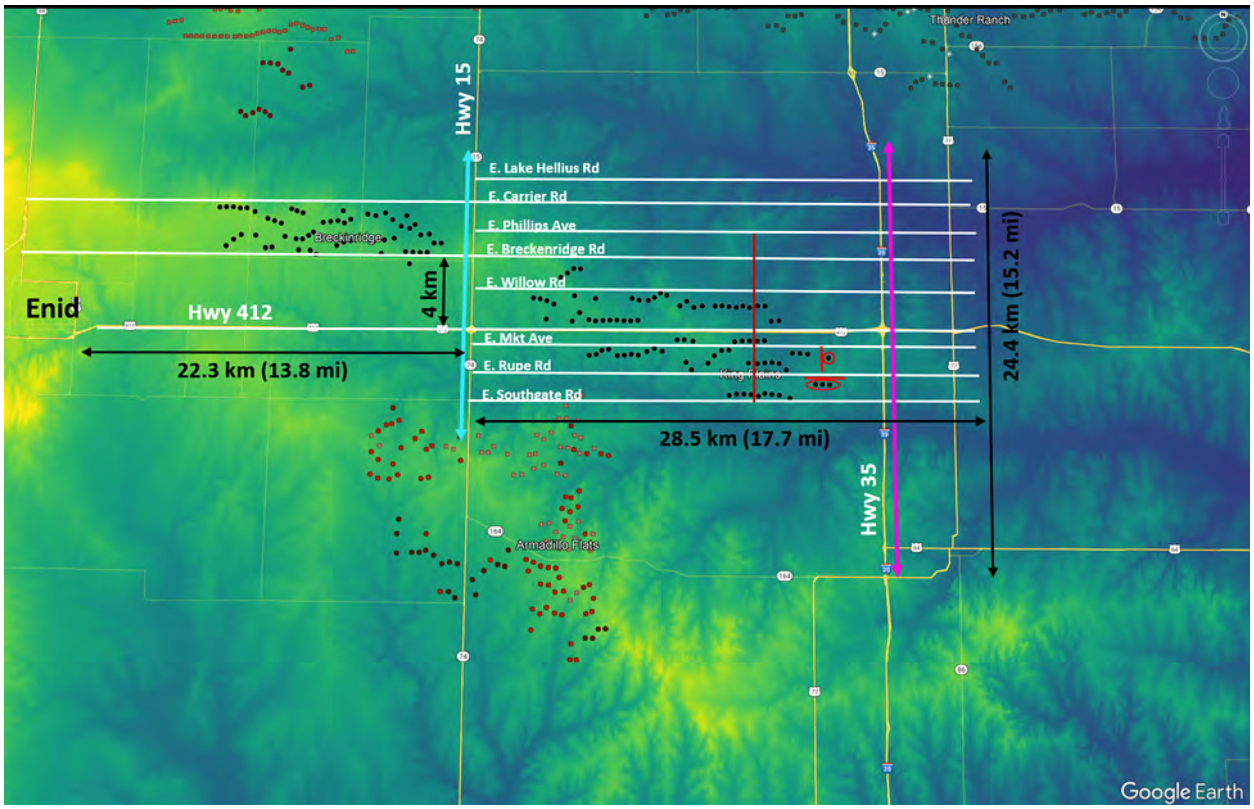

FIG. 10. Driving patterns of PUMAS during AWAKEN as a function of observed wind direction: white lines indicate southerly winds, the cyan line shows the major drives for the easterly winds, and the magenta line shows the major drives for the westerly winds. The dark red line represents the driving path along CR 40, where several AWAKEN lidars and other remote sensing instruments are located. Red circles indicate turbines selected for performing RHI scans for the (top) easterly and (bottom) southerly winds.

pioneering field experiments[37,42] but have yet to be quantified in great detail in the context of operational utility-scale wind plants. Capturing the behavior of turbulence within the interior rows of a wind farm is critical to understanding turbine response. Gathering experimental data of both inflow and turbine response of interior rows can help quantify how the two are correlated. Past studies have shown that applying wind farm control through wake steering reduces fatigue loads for interior turbines,[85–87] and AWAKEN will provide unique observations to further validate this result and assess its variability.

Anemometers placed at various heights across sites A1 and G, as well as the existing 90-m King Plains meteorological tower, are all important for quantifying the change in turbulence as wind propagates through the wind farm. Site G also has a thermodynamic profiler and hosted a temporary installation of tethersondes deployed over two one-week campaigns with a simultaneous deployment at A1. The tethersondes have sonic anemometers located at three different heights and a distributed fiber-optic temperature sensor that measures temperature every 0.5 m up to a range of 1.5 km AGL. Also, scanning lidars at site A1 and A5 are coordinated to perform synchronized, high-resolution, dual-Doppler stares within the King Plains wind farm to retrieve (lidar-derived) turbulence information within the plant. The nacelle-mounted lidars will be a valuable source of information to perform advanced reconstruction of second-order wind statistics (e.g., Refs. 88–90).

A suite of sensors is placed on three of the instrumented turbines (H05, G02, E06, Fig. 3) to provide accurate observations of structural loading response of major turbine components, as shown in Fig. 12. Strain gauges placed at the blade root of all three blades measure both edgewise and flapwise bending moments. Additional strain gauges are placed at the tower base, tower mid, and tower top to measure both side-to-side and fore-aft tower bending moments. This provides a better estimate of rotor thrust, which is an important input quantity for many wind turbine wake models. A final set of strain gauges is placed on the low-speed shaft to measure bending moments and torque, which are important for understanding turbine drivetrain reliability, fatigue, and load response. Several redundant instruments are installed to track key turbine parameters such as yaw heading and rotor azimuth position at a higher sample rate and accuracy than normally available from the controller.

D. Blockage

Wind plant blockage refers to a deceleration of winds approaching a wind plant,[11] similar to, but broader than, the induction zone effect of an individual turbine. Because blockage can reduce the inflow wind speed to a wind farm, it will lower power production more than wind farm loss models based solely on undisturbed upwind wind speeds predict. Analysis of offshore SCADA data estimate this

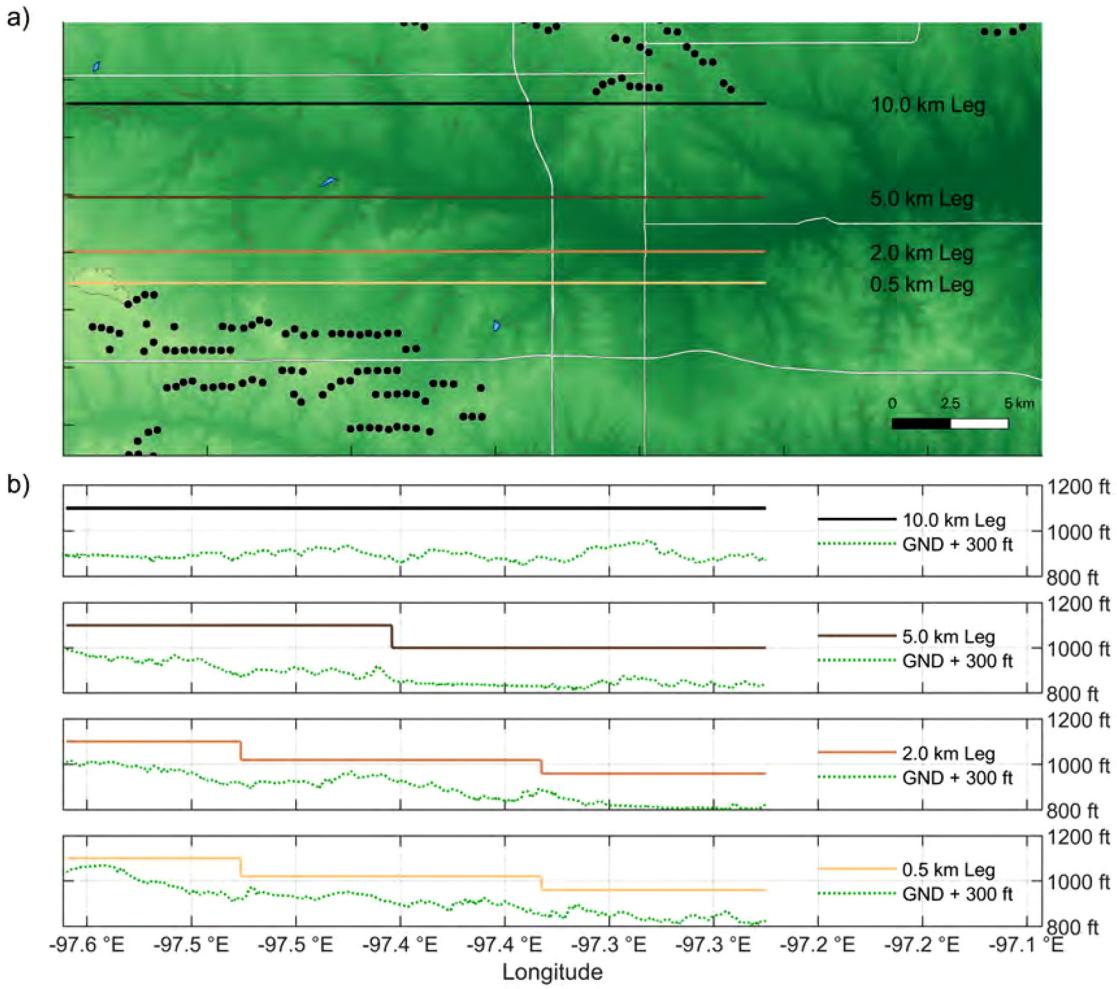

FIG. 11. (a) The measurement strategy for the aircraft measurements for southerly wind directions includes E–W transects located north of the King Plains wind plant, with increased spacing between the measurement legs (distance of 500 m, 2 km, 5 km, and 10 km alee of the northernmost row of turbines). (b) To ensure observations at approximately hub height with respect to the ground, steps in measurement altitude followed the terrain while maintaining the minimum granted altitude of 300 ft (ca. 91 m) above ground.

reduction as 2% of the Annual Energy Production (AEP),[91] with AEP reduction exceeding 6% for the turbines placed in the most upstream row.[12] However, the magnitude of the velocity reduction and the physical mechanisms inducing wind plant blockage are still poorly understood. Numerical[17,92] and experimental studies[93] indicate that blockage occurs more often in stably stratified conditions at high operating thrust coefficient (C_T). Other factors affecting the magnitude of blockage are the farm size[92,94] and layout.[17,94] The characterization of wind farm blockage through field experiments is challenged by terrain effects on flow,[13,95] extreme wind veer,[96] and high instrumental uncertainty compared to the magnitude of wind speed reduction.[93] The uncertainty of blockage measurement can be reduced by shutting down turbines, but this is costly to the wind farm operator.

Instruments placed at sites A1, A2, A5, and A7, as well as the nacelle-mounted lidars on turbine H05 and the X-band radars, are configured to observe the impacts of blockage upwind of the King Plains wind farm. The spatial distribution of these sites enables observations of both the spatial structure and temporal evolution of flow conditions upwind of the farm.

The key instruments for observing blockage effects are scanning and profiling lidars. As discussed in the inflow section, dual-Doppler scans are conducted using long-range scanning Doppler lidars at A5 and A7. The scans for each of these systems are coordinated in order to create a series of virtual towers at varying distances in front of the leading row turbines in the King Plains wind farm. The virtual towers are formed at the intersections of range-height-indicator (RHI) scans (i.e., a scan where the azimuth angle is kept constant, and the elevation angle varies), where profiles of wind speed and direction can be retrieved from dual-Doppler analysis of the radial velocity data.[65] This technique provides accurate estimates of two-dimensional winds,[97,98] and is not prone to the issues affecting the profiling lidars, e.g., in the case of flow inhomogeneity. The scans are designed to observe the

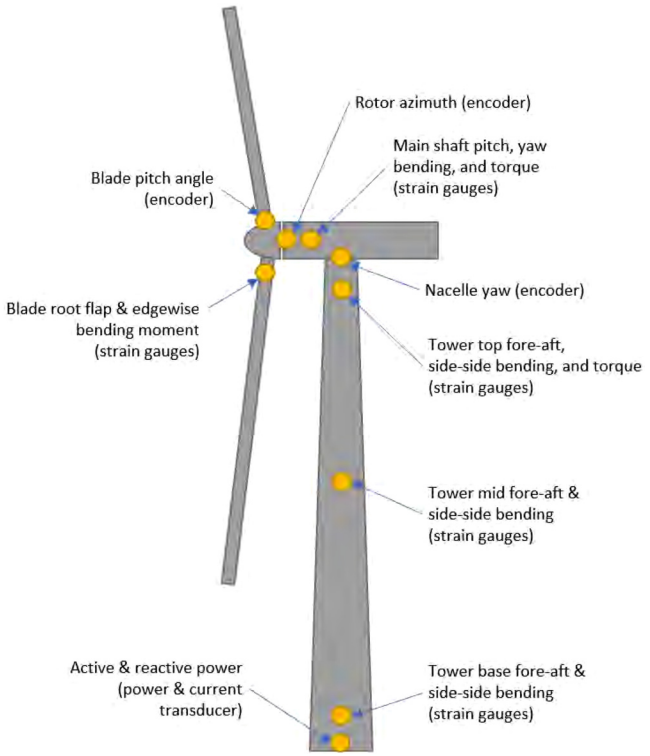

FIG. 12. Locations of additional sensors placed on wind turbines.

winds from the surface to approximately 300 m AGL at each of the virtual tower locations. These profiles provide important details on the evolution of the wind profile ahead of the Kings Plains wind farm and help quantify wind farm blockage effects.

In addition to the dual-Doppler lidar measurements, the thermodynamic profilers in the inflow help researchers identify the dependency of blockage on changing temperature profiles, and therefore local atmospheric static stability and ABL height. Nacelle-based lidars are also considered for blockage assessments, even though the difficulty of discerning the relatively subtle impact of blockage from the terrain-induced wind speed variations around King Plains and the inevitable dynamics of the nacelle tilt/roll could undermine the ability of nacelle-based scanning lidars to assess the phenomenon, especially if scanning horizontally.[13] For this reason, the scanning lidar installed on turbine H05 (Fig. 3) periodically performs a volumetric scan to reconstruct the 3D streamwise velocity up to 30*D* upstream of King Plains for southerly wind, enabling the detection of possible blockage.

Thrust-induced flow accelerations or speedups are phenomena related to blockage but still debated in the wind energy community. Theoretical,[99] numerical,[15,100,101] and also experimental results[102] indicate that substantial enhancements in power capture are attainable for closely spaced turbines thanks to the ensuing flow channeling effects, which have prompted some authors to explore the benefit of speedups to improve wind farm efficiency.[103] However, this argument runs counter to other studies that show no significant power increase.[12,94] To verify the presence of this phenomenon in the context of AWAKEN, the nacelle-mounted lidar placed on turbine G06 is devoted to the detection of flow acceleration and channeling effects at the southeastern boundary of King Plains, a location where speedups are more likely.[26] The lidar performs a full plan position indicator (PPI) scan (i.e., a scan where the elevation angle is kept constant, and the azimuth angle varies) specifically designed to reconstruct the mean flow at hub height at length scales relevant to the study of pressure-induced effects.

E. Wind farm control

One unique aspect of the AWAKEN project is the testing of wind farm control methods throughout a utility-sized wind plant. Two different types of wind farm controls are studied: wake steering[104–106] and consensus control.[107,108] Wake steering involves the yawing of upstream turbines to deflect their wakes away from downstream turbines, increasing total energy production despite losses from yaw misalignment at the upstream turbine. Consensus control combines wind direction measurements from a set of nearby turbines to determine the wind direction at the turbine of interest more accurately than the turbine's own wind vane; this consensus wind direction estimate, which provides a smoother wind direction signal that better represents the slowly varying wind direction experienced by the rotor, can then be used to improve the yaw control of the turbine. During the experiment, consensus control is tested on 26 turbines on the western half of the King Plains wind plant, whereas combined consensus control and wake steering is implemented on 15 turbines on the eastern half of the wind plant, as shown in Fig. 13. In addition to the turbine SCADA

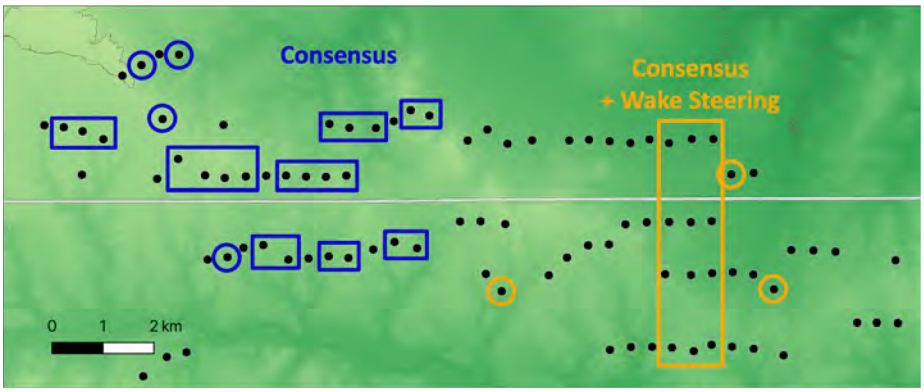

FIG. 13. King Plains wind turbines relevant for the wind plant control experimental activity.

data from all these turbines, inflow measurements of wind and temperature profiles upwind of King Plains as well as wake measurements from the scanning lidars (see Fig. 17) will also be used to help interpret the wind farm control results. Although several recent field experiments have been performed with wake steering controllers implemented on one or two wind turbines,[109–112] to our knowledge, this test represents the largest scale wind farm controls experiment to date.

In the consensus controller, a consensus wind direction is computed for each turbine using a weighted average of the wind direction signals from the turbine and its 12 nearest neighbors, similar to the approach presented by Sinner *et al.*[108] Note that the 12 nearest neighbors are used to determine the consensus wind direction regardless of whether they are operating with baseline, consensus, or combined consensus and wake steering control. Weights are based on the distance from each turbine to the turbine of interest using a Gaussian weighting function. Then, the consensus wind direction signal can effectively be used in place of the wind vane signal typically used for yaw control. The consensus wind direction signal is expected to provide a smoother, more accurate signal than a wind vane, which only measures the wind at a single point and is subjected to interference from the wind turbine nacelle and passing of the blades. Using neighboring turbines' signals essentially adds an element of spatial filtering to the wind direction signal used by the yaw controller. For this experiment, consensus yaw control is implemented by sending yaw offset commands to the turbines' existing yaw controllers to help orient the turbines toward their consensus wind directions rather than the turbines' individually measured wind directions. Each turbine's yaw offset command, which is updated every 10 s, is calculated as the difference between the 10-s average wind direction measured by the turbine's own wind vane and the 10-s average consensus wind direction.

The expected benefits of consensus control are as follows. When the consensus wind direction signal is used as an input to the individual wind turbine controller, as described above, the number of yaw activations of the turbine can be reduced because the yaw controller tracks a smoother wind direction reference; the reduced yaw activity can improve the reliability of the yaw system. Because of the anticipated higher accuracy of the consensus wind direction reference signal, wind direction tracking can likely be improved, leading to an increase in energy capture. Furthermore, using the consensus wind direction signal as an input to the wake steering controller provides it with a spatially averaged signal, rather than a local measurement, which can better represent the large-scale wind direction trends relevant to wind farm control, yielding more effective yaw offsets for wake steering. However, as suggested by Schepers *et al.*,[113] waked wind turbines can experience different wind directions than their upstream, unwaked counterparts because of the effects of partial wake impingement. Therefore, during the experiment, potential biases caused by including measurements from waked turbines in the consensus wind direction estimates are investigated.

The wake steering controller uses a lookup table to determine the target yaw offset for each wind turbine as a function of the consensus wind direction as well as the estimated freestream wind speed and plant-level turbulence intensity. The yaw misalignment setpoints of the turbines' yaw controllers are then changed to these yaw offsets, which are updated every 10 s. Whereas most wake steering controllers used in previous experiments include wind direction and wind speed to determine the yaw offsets, the strong dependence of wake steering performance on other atmospheric conditions, such as stability[114,115] and turbulence intensity (TI),[115,116] is addressed by including TI as a third dimension in the lookup table, similar to the controllers implemented by Doekemeijer *et al.*[110] and Howland *et al.*[112] Optimal yaw offsets are identified for each combination of wind direction (in steps of 1°), wind speed (in steps of 1 m/s), and TI (for values of 5%, 8%, 11%, 14%, and 17%) using NREL's computationally efficient FLOw Redirection and Induction in Steady State (FLORIS) wind farm control engineering tool[117] and the Serial-Refine method.[118] Yaw offsets for arbitrary combinations of wind direction, wind speed, and TI are found from the lookup table using linear interpolation. The yaw offset magnitude is constrained to be no more than 24° at low wind speeds, and the limit is reduced further as wind speed increases. Example yaw offsets from the lookup table are provided in Fig. 14 for the middle wind turbine in the second row from the south within the 12-turbine wake steering cluster.

The freestream wind speed input to the yaw offset lookup table is estimated as the mean wind speed measured by the set of 2–27 wind turbines classified as experiencing freestream inflow, depending on the median wind direction in the wind plant. The plant-level turbulence intensity is estimated at each time step as the 10th percentile of the measured TI values from the set of operating wind turbines, which are in turn calculated using 10-min statistics. The wind speed and plant-level turbulence intensity inputs to the lookup table are filtered using a first-order low-pass filter with a time constant of 60 s to better represent the slowly varying wind conditions relevant to wind farm control. Because the consensus wind direction input to the yaw offset lookup table already includes spatial and temporal averaging, as discussed earlier, no additional filtering is applied to this signal by the wake steering controller.

Wake steering can increase the yaw activity of the controlled turbines, which can accelerate damage to wind turbine components. Therefore, in addition to using the consensus wind direction estimates as inputs to the lookup table, consensus wind directions are also used as inputs to the turbines' standard yaw controllers to help reduce the overall number of yaw activations and yaw travel. Consensus control and wake steering are combined by summing the individual target yaw offsets determined for consensus control and wake steering. A high-level overview of the combined consensus and wake steering wind farm controller is shown in Fig. 15.

The consensus and wake steering controllers are evaluated during the experiment using a combination of controller toggling and comparison with reference wind turbines. For the consensus control experiment, which is tested on the western half of King Plains (see Fig. 13), 12 uniformly dispersed turbines, both on the outside and inside of the farm, are used as reference turbines throughout the campaign; they will still contribute their wind direction signal to neighbors but will only use their own wind vane signal for yaw control. The remaining 26 turbines are divided randomly into two halves every 30 min; one set of turbines will operate with a yaw controller that uses the consensus wind direction and the other will operate with the baseline control strategy. The random selection of turbines is intended to eliminate potential spatial sampling biases. Ideally, the toggling period would be minimized to eliminate temporal sampling effects, but since yaw controllers activate on the order of every 1–10 min, several yaw activations should be observed within each sampling period. To evaluate the

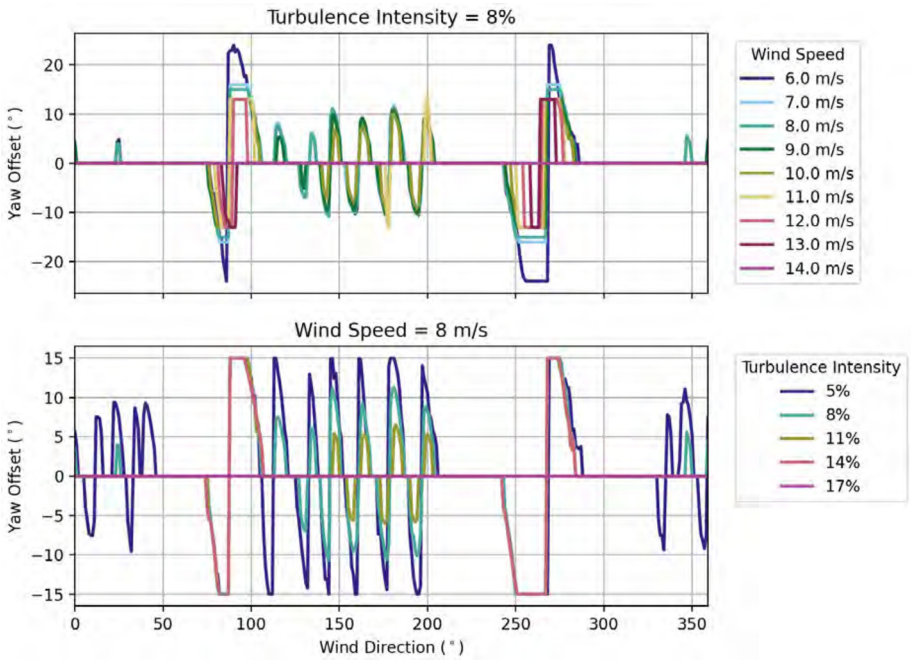

FIG. 14. Example yaw offsets for wake steering for the middle wind turbine in the second row from the south within the 12-turbine wake steering cluster shown in Fig. 13. The top plot shows the target yaw offsets as a function of wind speed for a turbulence intensity of 8%, and the bottom plot shows the yaw offsets as a function of turbulence intensity for a wind speed of 8 m/s.

impact of consensus control on the amount of yaw activity, yaw travel statistics for each turbine will be compared during baseline and consensus control periods. A similar process will be used to determine the impact of consensus control on energy production; however, the power production of each turbine will first be normalized by the average power of the reference turbines to help isolate the impact of the control strategy from factors that could affect the performance of all turbines in the wind plant, such as atmospheric conditions.

Wake steering is evaluated for 15 wind turbines on the eastern side of King Plains, including the 12 turbines in the 3×4 array shown in Fig. 13. Because these 12 turbines are separated by large distances [$\sim$10–15 rotor diameters (D)] for the predominant southerly wind directions, wake losses as well as energy gains from wake steering are expected to be relatively low, except during periods with low turbulence. To increase the likelihood of observing significant energy gains during the experiment, three additional turbines were selected for wake steering, with neighboring turbines only 4–8D downstream for southeasterly wind directions (see Fig. 13). The impact of wake steering on energy production and yaw activity is measured by toggling all 15 turbines hourly between baseline control and combined consensus and wake steering control so the two control modes can be evaluated in similar wind conditions. To avoid potential biases caused by implementing the same control mode at the same hour each day, the control mode selected for the first hour of the day will alternate. Similar to the consensus control experiment, yaw travel statistics and energy production will be compared for the two control modes to determine the impact of wake steering, with the power production of the test turbines normalized by the power of nearby wind direction-dependent freestream

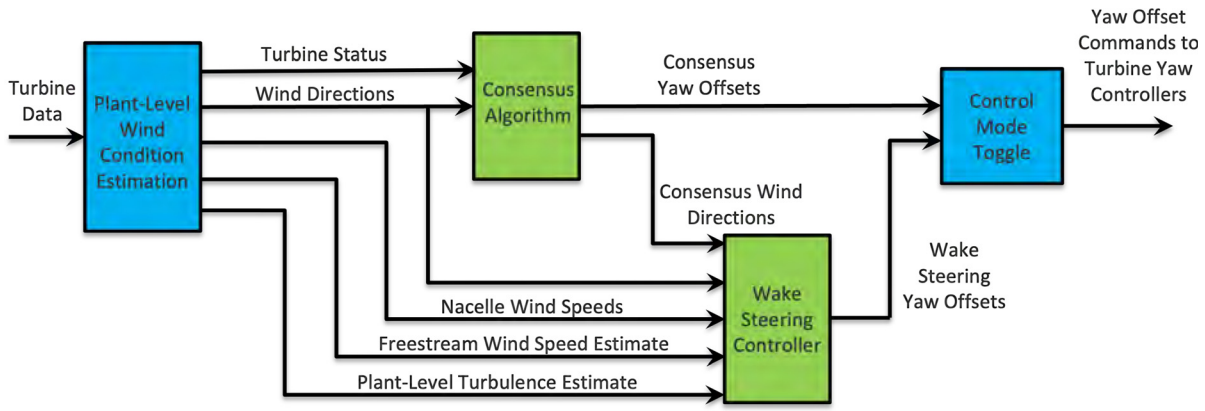

FIG. 15. Overview of the combined consensus and wake steering wind farm controller.

reference turbines. Note that the first 10–20 min after a control mode change should be discarded when analyzing the data to (1) provide time for the yaw controllers to adjust to the new yaw offset targets and (2) allow wakes influenced by the previous control mode to finish propagating through the cluster of test turbines.

F. Wind farm atmosphere momentum balance and intermittent turbulent events

Entrainment of momentum from the surrounding atmosphere is needed to replenish the wind resource within a wind farm and is especially critical for maximizing the power output from large wind farms. Observations have suggested that wake replenishment in the center of a wind farm is weaker than on the edges.[41] Over the last decade, large-eddy simulation studies[119–121] have examined entrainment from the atmospheric boundary layer into the wind farm boundary layer, in particular examining how farm layout and turbine spacing impact turbulence length scales and hence, entrainment. However, these modeling studies have typically employed idealized setups and therefore do not provide full insight into the wind farm–atmosphere momentum balance that prevails under realistic conditions. In particular, under stable conditions and when the wind farm boundary layer does not attain a fully developed state, it has been found that horizontal momentum fluxes can dominate over vertical entrainment as the chief means of replacing kinetic energy within the turbine array.[122] Recently, turbulent momentum fluxes and entrainment around large offshore wind farms were examined using aircraft-based observations,[123] notably revealing the significance of horizontal momentum fluxes under many conditions as well the profound impact of atmospheric stratification on the characteristics of momentum exchange between the wind farm and surrounding atmosphere. AWAKEN's observational strategy has detailed turbulence and thermodynamic profile observations available upstream (sites A1, A2, B, E36), downstream (site H), and lateral (site C1a, Golf Course) to the wind farm that allow these issues to be examined (Fig. 16)[124] for land-based wind farms in a region with strong atmospheric stability variations. Moreover, statistical analyses of power output and other operational data from the King Plains wind farm and the observed state of the wind farm-atmosphere momentum balance under different atmospheric conditions allows the validity of testable hypothesis 5 to be assessed.

Intermittent bursts of turbulence have been observed in the nocturnal boundary layer.[125–128] These bursts can originate on clear, moderately stable nights from a number of physical causes, including the breakdown of gravity waves,[126] from shear instability found underneath a low-level jet (LLJ)[125,129] or downslope flows,[130] from Kelvin–Helmholtz instabilities,[125,128] or from strong wind gusts aloft.[126,130] During AWAKEN, measurements of intermittent bursts of turbulence found in the rotor-disk layer (~25–160 m) will be taken using profiling and scanning lidars at sites A1, A2, B, C1a, and H. Additionally, E36 provides measurements of background intermittent turbulence at a location minimally influenced by the area's wind farms. In the WFAI context, key concerns associated with these intermittent turbulent events are their effects on power production and turbine structural loading. Thus, the load measurements from turbines H05, G02, and E06 can be scrutinized during periods of turbulence intermittency to evaluate testable hypothesis 7.

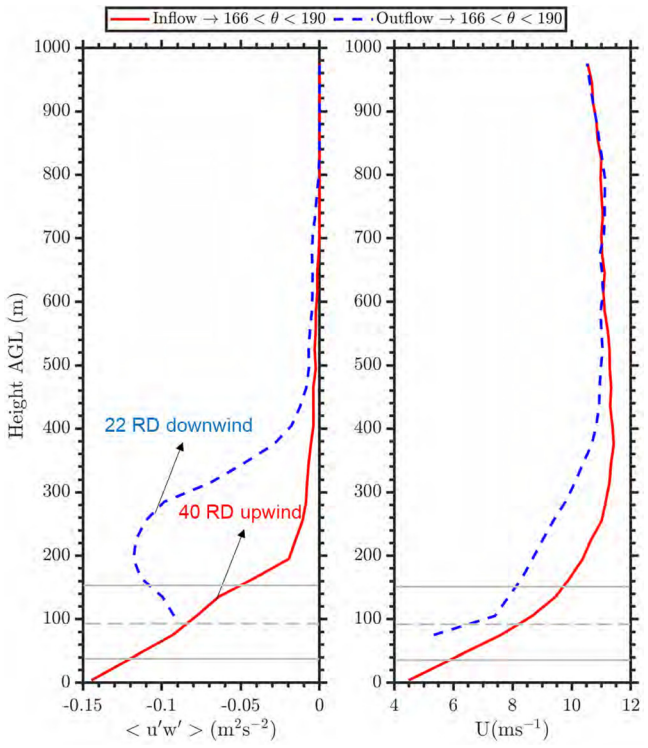

FIG. 16. Median momentum flux profiles (left) and median horizontal wind speed (right) from a surface sonic anemometer and a lidar at 40 D (or rotor diameters (RD)) upwind of King Plains (site A2) and a lidar at 22 D downwind (site H) during southerly wind directions (from 166° to 190°), from March 17, 2023, to September 10, 2023. The vertical limits of the wind turbine rotor layer are shown with gray continuous lines; dashed lines show the hub height.

G. Wind turbine wakes

Individual turbine wakes have been one of the most extensively studied flow features in wind energy research since they represent the major cause for power losses in large wind farms.[29,131,132] Although several mechanisms of wake dynamics are well-understood in controlled environmental conditions, only the recent advent of remote sensing technology has permitted the characterization of wakes from utility-scale generators placed in the ABL.[40–42,133–140] The cited studies generally focus on the characterization of wakes from a single turbine under undisturbed inflow, whereas there is a need to further investigate the behavior of internal wind farm wakes. The AWAKEN instruments have the capability to detect single and merging wakes, thus potentially expanding the knowledge of previous field studies. Furthermore, the wake characterization is instrumental to address other testable hypotheses, namely, those focusing on wind farm control, wake-generated turbulence, and farm wake.

Wind turbine wakes are primarily characterized by measurements from scanning lidars that have been mounted on the nacelle of five turbines within the King Plains wind plant (Fig. 17). Additional wake characterization is possible using the dual-Doppler wind fields generated by the Texas Tech X-band radar systems over large portions of the Armadillo Flats, Breckinridge, and King Plains wind plants (see Fig. 8).

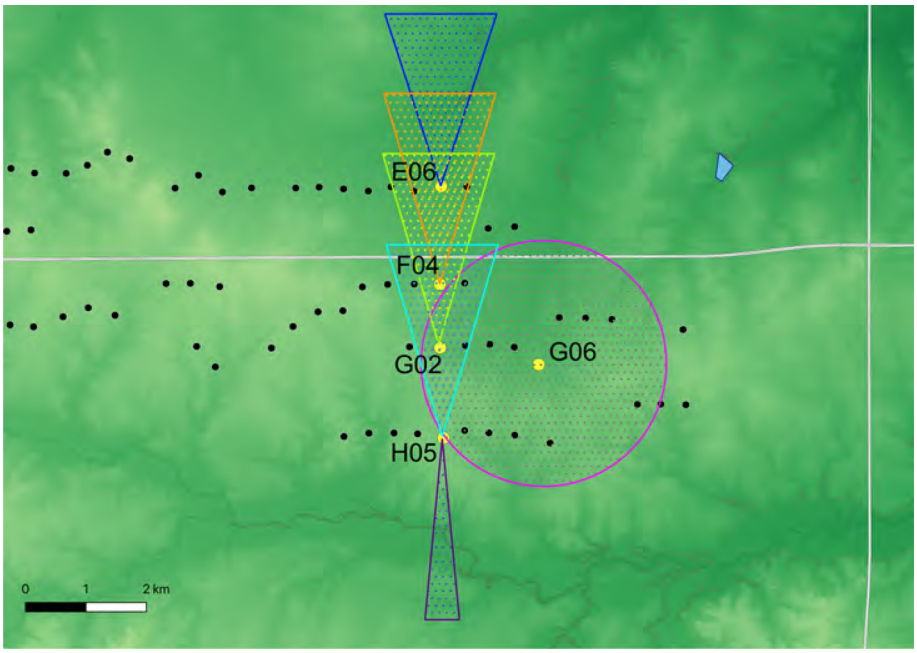

FIG. 17. King Plains turbines that have been instrumented with nacelle-mounted lidars, and qualitative sketches of the regions being scanned by each lidar.

The scanning lidars on the instrumented turbines H05, G02, F04, and E06 will be primarily used to characterize turbine wake variability. Having multiple nacelle-mounted lidars on a north-south transect allows for a systematic quantification of the turbine wakes at various downwind distances within the wind plant, as well as an assessment of the inflow conditions, given the predominant southerly wind direction (see Fig. 2). The lidars use a complex scanning strategy (see Letizia *et al.*[141] for details), which has been optimized with the LiDAR Statistical Barnes Objective Analysis (LiSBOA) tool proposed in Letizia *et al.*[89,142]

All scans have been designed to take into account the wake steering activities that involve the instrumented turbines, and the scanning strategy is differentiated between periods with and without wake steering misalignments. In general, the inflow is characterized by fast PPI horizontal scans. The variability of wind turbine wake statistics is assessed with a combination of slow PPI during wake steering and volumetric scans otherwise. Particular focus is given to wake meandering, whose quantification is achieved with a combination of both fast PPI and RHI scans. Redundant measurements for wake analysis are also provided by the nacelle-mounted staring lidar placed on H05 (primarily used for control purpose) and the lidar on G06, which performs 360° PPIs for the detection of speedups.

Figure 18 showcases a turbine wake analysis with volumetric lidar data from turbine E06. The mean streamwise velocity deficit undergoes drastic changes from one period to the next as a consequence of the changing wind conditions (high shear and veer onset after 0500 UTC) and power curtailment (0600-0800 UTC).

H. Precipitation measurements

Although not included in the formal list of testable hypotheses, the AWAKEN field campaign is also collecting data to better understand the relationship between wind plants, turbines, and precipitation. As such, laser disdrometers have been placed at sites A1 (near surface, data shown in Fig. 19), H (near surface), and on the nacelle of the turbine H05 to measure droplet size distribution and intensity.

These observations can be used to understand to what extent wind turbines and plants impact precipitation properties, in terms of variation of the spatial distribution of precipitation characteristics across a wind farm. Previous studies suggested either limited[143] or no[142] impacts on precipitation by wind farms. The observations collected at AWAKEN would represent the first ones to more definitively quantify the impacts of wind turbines on local precipitation patterns. Additionally, precipitation data will also be used for analysis to understand how impacts from hydrometeors leads to material stresses in wind turbine blades.[145] Leading-edge erosion (LEE) of wind-turbine blades is an important challenge that the wind industry is facing[146] and is a major cause of blade repair/replacement. LEE leads to structural degradation and poor aerodynamic performance, thereby affecting the power output of the turbines and increasing maintenance and repair costs. One of the main causes of LEE is attributed to multiple impacts from rain droplets and hailstones, which trigger wave propagation in the protective layers of the aerodynamic surface, leading to its degradation and erosion.[147] Higher tip speeds are one of the chief contributors to LEE since they largely dictate the closing velocities and thus impact kinetic energy transfer between the hydrometeors and the blade.[148] Reducing turbine blade tip speeds during high-rainfall events, the so-called "erosion safe" operating mode, has been found to significantly extend blade lifetimes.[145,149] Other mitigation strategies include leading-edge protection through tapes and coatings, though they require regular maintenance to preserve their effectiveness. Improving the predictive capabilities of LEE models can help to optimize maintenance and turbine operation schedules to extend blade lifetimes. Using precipitation data collected at multiple heights (surface and hub-height) and surrounding a wind farm (inflow and within) will permit

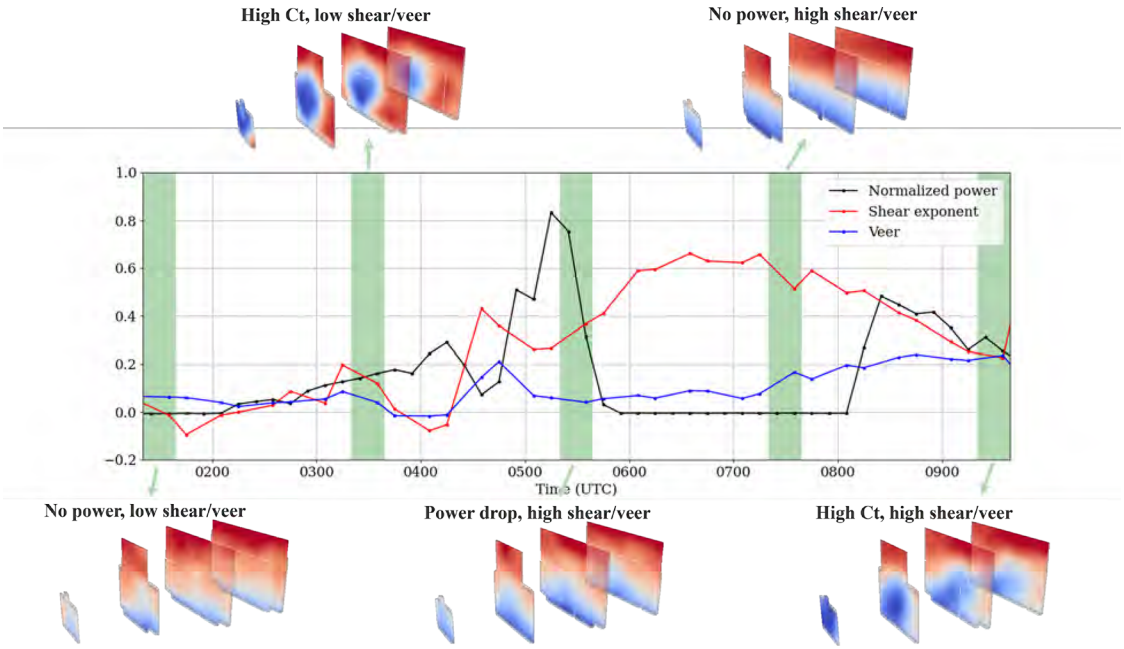

FIG. 18. Case study of 3D wake mean velocity evolving throughout a period of transitional wind conditions and wind farm curtailment. Shaded areas indicate the availability of volumetric scans within the scanning schedules.

quantification of the combined effect of precipitation impact and wake-induced turbulence on LEE.

V. DATA MANAGEMENT

The AWAKEN project will produce the largest quality-controlled experimental, multi-instrumental dataset describing wind farm–atmosphere interactions to date. Given the size and unique nature of this dataset, our data management practices adhere to findability, accessibility, interoperability, and reusability (FAIR) principles[150] to maximize the utility of this dataset for atmospheric science and wind energy researchers and the return on investment for all project partners and funding agencies. To this end, we will store and broadly disseminate all data in the public domain on two fronts: the ARM Data Center (https://adc.arm.gov) and the DOE Atmosphere to Electrons Wind Data Hub (https://a2e.energy.gov).[151] As detailed in the main instrumentation timeline spreadsheet hosted on the Wind Data Hub AWAKEN project page, the ARM Data Center is the primary hub to host observations from ARM-owned instruments, whereas the Wind Data Hub is the main portal for data from all remaining instruments.

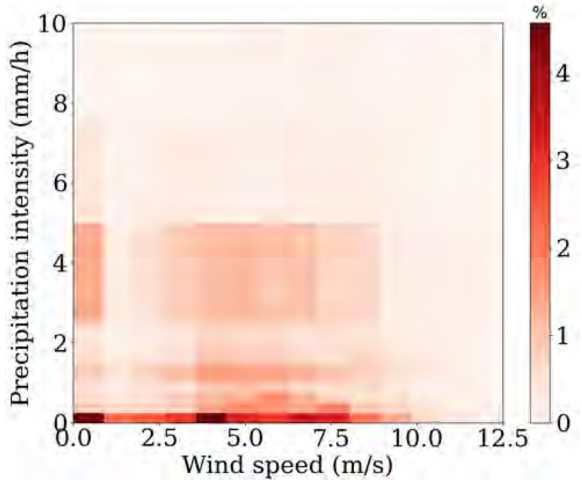

FIG. 19. Joint probability distributions between wind speed and rain intensity at site A1 from January 1, 2023, to September 10, 2023.

The Wind Data Hub upload procedure includes execution of the following automated processes: (1) data standardization to NetCDF format, (2) basic preprocessing of raw data to calculate thermo-fluid-mechanic quantities of interest, (3) quality assurance and preliminary quality control, (4) verification of metadata completeness, and (5) assignment of a unique digital object identifier (DOI). All data from the ground sites are public and made available to registered users, and archived in the long term, with metadata stored in perpetuity.

VI. CONCLUSIONS

AWAKEN is a unique field campaign to gather new observations of WFAI that will be useful for the wind industry and research community alike. These observations will include new observations of wind farm and turbine wakes, structural loading impacts from atmospheric and wake turbulence, low-level jet impacts on performance and large-scale testing of two wind farm controls technologies. The field campaign has been designed to optimize placement and operation of instruments around a series of five wind farms in Northern Oklahoma. These instruments provide observations that researchers will use to address seven testable hypotheses, identified as key research

priorities by wind energy experts. The data gathered will be used to validate and improve simulation tools that will be used for future wind farm layout optimization and wind farm control design. Most of the observations will be publicly available in DOE's Wind Data Hub. Lessons learned from this project will advance the current state of the art in wind energy science, help industry lower the cost of wind energy, and inform future field campaigns on further WFAI data needs, both on land and offshore.

ACKNOWLEDGMENTS

This work was authored in part by the National Renewable Energy Laboratory, operated by Alliance for Sustainable Energy, LLC, for the U.S. Department of Energy under Contract No. DE-AC36-08GO28308. Additional work was performed under the auspices of the U.S. Department of Energy by Lawrence Livermore National Laboratory under Contract No. DE-AC52-07NA27344 and Pacific Northwest National Laboratory. PNNL is operated by Battelle Memorial Institute for the Department of Energy under Contract No. DE-AC05-76RL01830. Sandia National Laboratories is a multimission laboratory managed and operated by National Technology & Engineering Solutions of Sandia, LLC, a wholly owned subsidiary of Honeywell International Inc., for the U.S. Department of Energy's National Nuclear Security Administration under Contract No. DE-NA0003525. Funding was provided by the U.S. Department of Energy Office of Energy Efficiency and Renewable Energy Wind Energy Technologies Office. This paper describes objective technical results and analysis. Any subjective views or opinions that might be expressed in the paper do not necessarily represent the views of the U.S. Department of Energy or the U.S. Government. The U.S. Government retains, and the publisher, by accepting the article for publication, acknowledges that the U.S. Government retains a nonexclusive, paid-up, irrevocable, worldwide license to publish or reproduce the published form of this work, or allow others to do so, for U.S. Government purposes. The participation of the research aircraft of TU Braunschweig was funded by the Klaus Tschira Stiftung gGmbH (Germany) under Contract No. 03.006.2023. The provision of one scanning lidar and one profiling lidar was financed by the German Federal Ministry for Economic Affairs and Climate Action (BMWK) as part of the project Windpark Radar (Funding Code 03EE3031A). (Some) data were obtained from and this research was supported by the Atmospheric Radiation Measurement (ARM) user facility, a U.S. Department of Energy (DOE) Office of Science user facility managed by the Biological and Environmental research program.

The authors would like to thank the AWAKEN site landowners (Harvey Hentges, Rocky Honeywell, Tony Lee, Alvin Mayer, William North, Rick Oller, Joe Surface, Mark and Stacie Wade, Elizabeth Chaloupek) and their families. We also thank the community members of Enid and surrounding towns for their support throughout the field campaign. The successful commencement of this campaign is greatly indebted to the tireless students and technicians who helped prepare the AWAKEN sites and deploy instruments. Finally, we thank our project partners at ARM SGP, ENGIE, GE, Enel, and NextEra for their continuous support. We also thank LRTech, Lumibird, Vaisala, and other instrument manufacturers for providing support throughout the field experiment.

AUTHOR DECLARATIONS

Conflict of Interest

The authors have no conflicts to disclose.

Author Contributions

Patrick Moriarty: Conceptualization (equal); Funding acquisition (equal); Project administration (equal); Supervision (equal); Writing – original draft (equal); Writing – review & editing (equal). **Nicola Bodini:** Conceptualization (equal); Investigation (equal); Methodology (equal); Writing – original draft (equal); Writing – review & editing (equal). **Stefano Letizia:** Conceptualization (equal); Methodology (equal); Writing – original draft (equal); Writing – review & editing (equal). **Aliza Abraham:** Data curation (equal); Formal analysis (equal); Validation (equal); Writing – review & editing (equal). **Tyler Ashley:** Investigation (equal); Resources (equal). **Konrad Bärfuss:** Conceptualization (equal); Data curation (equal); Methodology (equal). **Rebecca Barthelmie:** Conceptualization (equal); Data curation (equal); Investigation (equal). **Alan Brewer:** Data curation (equal); Formal analysis (equal); Methodology (equal); Resources (equal). **Peter Brugger:** Methodology (equal); Writing – original draft (equal). **Thomas Feuerle:** Conceptualization (equal); Investigation (equal); Methodology (equal). **Ariane Frère:** Conceptualization (equal); Investigation (equal); Methodology (equal); Project administration (equal). **Lexie Goldberger:** Methodology (equal); Writing – original draft (equal). **Julia Gottschall:** Conceptualization (equal); Investigation (equal). **Nicholas Hamilton:** Conceptualization (equal); Methodology (equal); Writing – original draft (equal); Writing – review & editing (equal). **Thomas Herges:** Conceptualization (equal); Writing – review & editing (equal). **Brian Hirth:** Conceptualization (equal); Writing – original draft (equal). **Lin-Ya (Lilian) Hung:** Conceptualization (equal); Investigation (equal). **Giacomo Valerio Iungo:** Conceptualization (equal); Methodology (equal); Writing – original draft (equal). **Chris Ivanov:** Methodology (equal); Writing – original draft (equal). **Colleen Kaul:** Conceptualization (equal); Methodology (equal); Writing – original draft (equal); Writing – review & editing (equal). **Stefan Kern:** Funding acquisition (equal); Methodology (equal); Visualization (equal). **Petra Klein:** Conceptualization (equal); Methodology (equal). **Raghavendra Krishnamurthy:** Conceptualization (equal); Methodology (equal); Writing – original draft (equal). **Astrid Lampert:** Conceptualization (equal); Investigation (equal); Methodology (equal). **Julie K. Lundquist:** Conceptualization (equal); Methodology (equal); Writing – original draft (equal). **Victor R. Morris:** Methodology (equal). **Rob Newsom:** Conceptualization (equal); Methodology (equal); Writing – original draft (equal). **Mikhail Pekour:** Conceptualization (equal); Methodology (equal). **Yelena Pichugina:** Conceptualization (equal); Formal analysis (equal); Investigation (equal). **Fernando Porte-Agel:** Conceptualization (equal); Funding acquisition (equal); Methodology (equal). **Sara C. Pryor:** Conceptualization (equal); Investigation (equal). **Andrew Scholbrock:** Conceptualization (equal); Methodology (equal). **John Schroeder:** Conceptualization (equal); Methodology (equal). **Samuel Shartzer:** Conceptualization (equal); Formal analysis (equal); Funding acquisition (equal); Investigation (equal). **Eric Simley:** Conceptualization (equal); Investigation (equal); Writing – original draft (equal). **Lilén Vöhringer:** Conceptualization (equal); Investigation

(equal). **Sonia Wharton:** Conceptualization (equal); Methodology (equal); Writing – original draft (equal). **Daniel Zalkind:** Conceptualization (equal); Methodology (equal); Writing – original draft (equal).

DATA AVAILABILITY

The data that support the findings of this study are openly available at https://a2e.energy.gov/project/awaken, Ref. 152.

REFERENCES

[1]A. Clifton, A. D. Smith, and M. J. Fields, "Wind plant preconstruction energy estimates. Current practice and opportunities," Technical Report No. NREL/TP-5000-64735 [National Renewable Energy Laboratory (NREL), Golden, Colorado, 2016].

[2]J. C. Y. Lee and M. J. Fields, "An overview of wind-energy-production prediction bias, losses, and uncertainties," Wind Energy Sci. **6**, 311–365 (2021).

[3]S. C. Pryor, T. J. Shepherd, P. J. H. Volker, A. N. Hahmann, and R. J. Barthelmie, ""Wind theft" from onshore wind turbine arrays: Sensitivity to wind farm parameterization and resolution," J. Appl. Meteorol. Climatol. **59**, 153–174 (2020).

[4]F. Porté-Agel, M. Bastankhah, and S. Shamsoddin, "Wind-turbine and wind-farm flows: A review," Boundary-Layer Meteorol. **174**, 1–59 (2020).

[5]J. K. Lundquist, K. K. DuVivier, D. Kaffine, and J. M. Tomaszewski, "Costs and consequences of wind turbine wake effects arising from uncoordinated wind energy development," Nat. Energy **4**, 26–34 (2019).

[6]J. Meyers, C. Bottasso, K. Dykes, P. Fleming, P. Gebraad, G. Giebel, T. Göçmen, and J.-W. van Wingerden, "Wind farm flow control: Prospects and challenges," Wind Energy Sci. **7**, 2271 (2022).

[7]D. R. Houck, "Review of wake management techniques for wind turbines," Wind Energy **25**, 195 (2021).

[8]AWS Truepower, *Openwind Theoretical Basis and Validation, Version 1.3* (AWS Truepower, Albany, New York, 2010).

[9]A. Crespo, J. Hernandez, and S. Frandsen, "Survey of modelling methods for wind turbine wakes and wind farms," Wind Energy **2**, 1–24 (1999).

[10]T. Göçmen, P. Van der Laan, P.-E. Réthoré, A. P. Diaz, G. C. Larsen, and S. Ott, "Wind turbine wake models developed at the technical university of Denmark: A review," Renewable Sustainable Energy Rev. **60**, 752–769 (2016).

[11]J. Bleeg, M. Purcell, R. Ruisi, and E. Traiger, "Wind farm blockage and the consequences of neglecting its impact on energy production," Energies **11**, 1609 (2018).

[12]N. G. Nygaard, S. T. Steen, L. Poulsen, and J. G. Pedersen, "Modelling cluster wakes and wind farm blockage," J. Phys. **1618**, 062072 (2020).

[13]M. Sanchez Gomez, J. K. Lundquist, J. D. Mirocha, R. S. Arthur, D. Muñoz-Esparza, and R. Robey, "Can lidars assess wind plant blockage in simple terrain? A WRF-LES study," J. Renewable Sustainable Energy **14**, 063303 (2022).

[14]P. Moriarty and T. Kogaki, "Modeling of flow acceleration around wind farms," in ASME/JSME 5th Joint Fluids Engineering Conference, 2007.

[15]A. R. Meyer Forsting, N. Troldborg, and M. Gaunaa, "The flow upstream of a row of aligned wind turbine rotors and its effect on power production," Wind Energy **20**, 63–77 (2017).

[16]S. Frandsen, R. Barthelmie, S. Pryor, O. Rathmann, S. Larsen, J. Højstrup, and M. Thøgersen, "Analytical modelling of wind speed deficit in large offshore wind farms," Wind Energy **9**, 39–53 (2006).

[17]K. L. Wu and F. Porté-Agel, "Flow adjustment inside and around large finite-size wind farms," Energies **10**, 2164 (2017).

[18]S. K. Siedersleben, A. Platis, J. K. Lundquist, B. Djath, A. Lampert, K. Bärfuss, B. Cañadillas, J. Schulz-Stellenfleth, J. Bange, T. Neumann, and S. Emeis, "Turbulent kinetic energy over large offshore wind farms observed and simulated by the mesoscale model WRF (3.8.1)," Geosci. Model Dev. **13**, 249–268 (2020).

[19]R. J. A. M. Stevens and C. Meneveau, "Flow structure and turbulence in wind farms," Annu. Rev. Fluid Mech. **49**, 311 (2017).

[20]M. A. Sprague, S. Ananthan, G. Vijayakumar, and M. Robinson, "ExaWind: A multifidelity modeling and simulation environment for wind energy," J. Phys. **1452**, 012071 (2020).

[21]P. Moriarty, N. Hamilton, M. Debnath, T. Herges, B. Isom, J. K. Lundquist, D. Maniaci, B. Naughton, R. Pauly, J. Roadman, W. Shaw, J. van Dam, and S. Wharton, "American WAKE experimeNt (AWAKEN)," Technical Report No. NREL/TP-5000-75789 [National Renewable Energy Laboratory (NREL), Golden, CO, 2020].

[22]M. Debnath, A. K. Scholbrock, D. Zalkind, P. Moriarty, E. Simley, N. Hamilton, C. Ivanov, R. S. Arthur, R. Barthelmie, N. Bodini, A. Brewer, L. Goldberger, T. Herges, B. Hirth, G. V. Iungo, D. Jager, C. Kaul, P. Klein, R. Krishnamurthy, S. Letizia, J. K. Lundquist, D. Maniaci, R. Newsom, M. Pekour, S. C. Pryor, M. T. Ritsche, J. Roadman, J. Schroeder, W. J. Shaw, J. V. Dam, and S. Wharton, "Design of the American Wake Experiment (AWAKEN) field campaign," J. Phys. **2265**, 022058 (2022).

[23]R. J. Barthelmie, M. S. Courtney, J. Højstrup, and S. E. Larsen, "Meteorological aspects of offshore wind energy: Observations from the Vindeby wind farm," J. Wind Eng. Ind. Aerodyn. **62**, 191–211 (1996).

[24]J. Cleijne, "Results of Sexbierum wind farm; double measurements," Technical Report TNO Report 92-388 (TNO, Netherlands, 1992).

[25]J. Cleijne, "Results of Sexbierum wind farm; single wake measurements," Technical Report TNO Report 93-082 (TNO, Netherlands, 1993).

[26]R. J. Barthelmie and L. E. Jensen, "Evaluation of wind farm efficiency and wind turbine wakes at the Nysted offshore wind farm," Wind Energy **13**, 573–586 (2010).

[27]R. J. Barthelmie, S. T. Frandsen, O. Rathmann, K. S. Hansen, E. Politis, J. Prospathopoulos, J. G. Schepers, K. Rados, D. Cabezón, W. Schlez *et al.*, "Flow and wakes in large wind farms: Final report for upwind WP8," Technical Report No. Risø-R-1765(EN) (Danmarks Tekniske Universitet, Risø Nationallaboratoriet for Baeredygtig Energi, 2011).

[28]K. S. Hansen, R. J. Barthelmie, L. E. Jensen, and A. Sommer, "The impact of turbulence intensity and atmospheric stability on power deficits due to wind turbine wakes at Horns Rev wind farm," Wind Energy **15**, 183–196 (2012).

[29]R. J. Barthelmie, S. T. Frandsen, K. Hansen, J. G. Schepers, K. Rados, W. Schlez, A. Neubert, L. E. Jensen, and S. Neckelmann, "Modelling the impact of wakes on power output at Nysted and Horns Rev," in European Wind Energy Conference, 2009.

[30]M. Gaumond, P.-E. Réthoré, S. Ott, A. Pena, A. Bechmann, and K. S. Hansen, "Evaluation of the wind direction uncertainty and its impact on wake modeling at the Horns Rev offshore wind farm," Wind Energy **17**, 1169–1178 (2014).

[31]Y.-T. Wu and F. Porté-Agel, "Modeling turbine wakes and power losses within a wind farm using LES: An application to the Horns Rev offshore wind farm," Renewable Energy **75**, 945–955 (2015).

[32]S. El-Asha, L. Zhan, and G. V. Iungo, "Quantification of power losses due to wind turbine wake interactions through SCADA, meteorological and wind LiDAR data," Wind Energy **20**, 1823–1839 (2017).

[33]P. Moriarty, J. S. Rodrigo, P. Gancarski, M. Chuchfield, J. W. Naughton, K. S. Hansen, E. Machefaux, E. Maguire, F. Castellani, L. Terzi *et al.*, "IEA-Task 31 WAKEBENCH: Towards a protocol for wind farm flow model evaluation. Part 2: Wind farm wake models," J. Phys. **524**, 012185 (2014).

[34]R. J. Barthelmie, K. S. Hansen, and S. C. Pryor, "Meteorological controls on wind turbine wakes," Proc. IEEE **101**, 1010–1019 (2013).

[35]R. J. Barthelmie, G. Larsen, S. Frandsen, L. Folkerts, K. Rados, S. Pryor, B. Lange, and G. Schepers, "Comparison of wake model simulations with offshore wind turbine wake profiles measured by sodar," J. Atmos. Oceanic Technol. **23**, 888–901 (2006).

[36]H. Wang, R. J. Barthelmie, A. Clifton, and S. C. Pryor, "Wind measurements from arc scans with Doppler wind lidar," J. Atmos. Oceanic Technol. **32**, 2024–2040 (2015).

[37]B. D. Hirth, J. L. Schroeder, W. S. Gunter, and J. G. Guynes, "Measuring a utility-scale turbine wake using the TTUKa mobile research radars," J. Atmos. Oceanic Technol. **29**, 765–771 (2012).

[38]D. A. Rajewski, E. S. Takle, J. K. Lundquist, S. Oncley, J. H. Prueger, T. W. Horst, M. E. Rhodes, R. Pfeiffer, J. L. Hatfield, K. K. Spoth, and R. K. Doorenbos, "Crop Wind Energy Experiment (CWEX): Observations of surface-layer, boundary layer, and mesoscale interactions with a wind farm," Bull. Am. Meteorol. Soc. **94**, 655–672 (2013).

[39]G. V. Iungo, Y.-T. Wu, and F. Porté-Agel, "Field measurements of wind turbine wakes with lidars," J. Atmos. Oceanic Technol. **30**, 274–287 (2013).

[40]M. L. Aitken, R. M. Banta, Y. L. Pichugina, and J. K. Lundquist, "Quantifying wind turbine wake characteristics from scanning remote sensor data," J. Atmos. Oceanic Technol. **31**, 765–787 (2014).
[41]N. Bodini, D. Zardi, and J. K. Lundquist, "Three-dimensional structure of wind turbine wakes as measured by scanning lidar," Atmos. Meas. Tech. **10**, 2881–2896 (2017).
[42]L. Zhan, S. Letizia, and G. V. Iungo, "LiDAR measurements for an onshore wind farm: Wake variability for different incoming wind speeds and atmospheric stability regimes," Wind Energy **23**, 501–527 (2019).
[43]M. B. Christiansen and C. B. Hasager, "Wake effects of large offshore wind farms identified from satellite SAR," Remote Sens. Environ. **98**, 251–268 (2005).
[44]B. Cañadillas, R. Foreman, V. Barth, S. Siedersleben, A. Lampert, A. Platis, B. Djath, J. Schulz-Stellenfleth, J. Bange, S. Emeis, and T. Neumann, "Offshore wind farm wake recovery: Airborne measurements and its representation in engineering models," Wind Energy **23**, 1249–1265 (2020).
[45]B. Cañadillas, M. Beckenbauer, J. J. Trujillo, M. Dörenkämper, R. Foreman, T. Neumann, and A. Lampert, "Offshore wind farm cluster wakes as observed by long-range-scanning wind lidar measurements and mesoscale modeling," Wind Energy Sci. **7**, 1241–1262 (2022).
[46]A. Platis, J. Bange, K. Bärfuss, B. Cañadillas, M. Hundhausen, B. Djath, A. Lampert, J. Schulz-Stellenfleth, S. Siedersleben, T. Neumann, and S. Emeis, "Long-range modifications of the wind field by offshore wind parks—Results of the project WIPAFF," Meteorol. Z. **29**, 355–376 (2020).
[47]A. Platis, M. Hundhausen, A. Lampert, S. Emeis, and J. Bange, "The role of atmospheric stability and turbulence in offshore wind-farm wakes in the German Bight," Boundary-Layer Meteorol. **182**, 441–469 (2022).
[48]N. G. Nygaard and A. C. Newcombe, "Wake behind an offshore wind farm observed with dual-Doppler radars," J. Phys. **1037**, 072008 (2018).
[49]N. Wildmann, M. Hagen, and T. Gerz, "Enhanced resource assessment and atmospheric monitoring of the research wind farm WiValdi," J. Phys. **2265**, 022029 (2022).
[50]D. Turner and R. Ellingson, *The Atmospheric Radiation Measurement (ARM) Program: The First 20 Years* (American Meteorological Society, 2017).
[51]D. L. Sisterson, R. A. Peppler, T. S. Cress, P. J. Lamb, and D. D. Turner, "The Arm Southern Great Plains (SGP) site," Meteorol. Monogr. **57**, 6.1–6.14 (2016).
[52]See https://www.eia.gov/opendata/v1/qb.php?category=902967 for "Electricity Plan Level Data for Oklahoma" (last accessed December 30, 2022).
[53]B. D. Hoen, J. E. Diffendorfer, J. T. Rand, L. A. Kramer, C. P. Garrity, and H. E. Hunt, 2018 "United States Wind Turbine Database v6.0 (May 31, 2023)," U.S. Geological Survey, American Clean Power Association, and Lawrence Berkeley National Laboratory data release (accessed November 3, 2023).
[54]R. Krishnamurthy, R. K. Newsom, D. Chand, and W. J. Shaw, "Boundary layer climatology at ARM southern great plains," Technical Report No. PNNL-30832 [Pacific Northwest National Lab. (PNNL), Richland, WA, 2021].
[55]S. Wharton, M. Simpson, J. L. Osuna, J. F. Newman, and S. C. Biraud, "Role of surface energy exchange for simulating wind turbine inflow: A case study in the southern great plains, USA," Atmosphere **6**, 21–49 (2014).
[56]N. Bodini, J. K. Lundquist, and P. Moriarty, "Wind plants can impact long-term local atmospheric conditions," Sci. Rep. **11**, 22939 (2021).
[57]A. Sathe and J. Mann, "Measurement of turbulence spectra using scanning pulsed wind lidars," J. Geophys. Res. **117**, D01201, https://doi.org/10.1029/2011JD016786 (2012).
[58]J. F. Newman, P. M. Klein, S. Wharton, A. Sathe, T. A. Bonin, P. B. Chilson, and A. Muschinski, "Evaluation of three lidar scanning strategies for turbulence measurements," Atmos. Meas. Tech. **9**, 1993–2013 (2016).
[59]A. Sathe, J. Mann, N. Vasiljevic, and G. Lea, "A six-beam method to measure turbulence statistics using ground-based wind lidars," Atmos. Meas. Tech. **8**, 729–740 (2015).
[60]W. L. Eberhard, R. E. Cup, and K. R. Healy, "Doppler LiDAR measurement of profiles of turbulence and momentum flux," J. Atmos. Oceanic Technol. **6**, 809–819 (1989).
[61]N. Hamilton and M. Debnath, "National Wind Technology Center–Characterization of Atmospheric Conditions," Technical Report No. NREL/TP-5000-72091 (National Renewable Energy Laboratory, Golden, CO, 2019).
[62]D. D. Turner and U. LöHnert, "Information content and uncertainties in thermodynamic profiles and liquid cloud properties retrieved from the ground-based Atmospheric Emitted Radiance Interferometer (AERI)," J. Appl. Meteorol. Climatol. **53**, 752–771 (2014).
[63]T. J. Wagner, P. M. Klein, and D. D. Turner, "A new generation of ground-based mobile platforms for active and passive profiling of the boundary layer," Bull. Am. Meteorol. Soc. **100**, 137–153 (2019).
[64]M. Debnath, G. V. Iungo, W. A. Brewer, A. Choukulkar, R. Delgado, S. Gunter, J. K. Lundquist, J. L. Schroeder, J. M. Wilczak, and D. Wolfe, "Assessment of virtual towers performed with scanning wind lidars and Ka-band radars during the XPIA experiment," Atmos. Meas. Tech. **10**, 1215–1227 (2017).
[65]R. Calhoun, W. R. R. Heap, P. Phelan, M. Princevac, R. K. Newsom, H. Fernando, and D. Ligon, "Virtual towers using coherent Doppler lidar during Joint Urban 2003 dispersion experiment," J. Appl. Meteorol. Climatol. **45**, 1116–1126 (2006).
[66]A. Platis, S. K. Siedersleben, J. Bange, A. Lampert, K. Bärfuss, R. Hankers, B. Cañadillas, R. Foreman, J. Schulz-Stellenfleth, B. Djath, T. Neumann, and S. Emeis, "First *in situ* evidence of wakes in the far field behind offshore wind farms," Sci. Rep. **8**, 2163 (2018).
[67]A. C. Fitch, J. K. Lundquist, and J. B. Olson, "Mesoscale influences of wind farms throughout a diurnal cycle," Mon. Weather Rev. **141**, 2173–2198 (2013).
[68]J. M. Tomaszewski and J. K. Lundquist, "Simulated wind farm wake sensitivity to configuration choices in the Weather Research and Forecasting model version 3.8.1," Geosci. Model Dev. **13**, 2645–2662 (2020).
[69]A. Rybchuk, T. W. Juliano, J. K. Lundquist, D. Rosencrans, N. Bodini, and M. Optis, "The sensitivity of the Fitch wind farm parameterization to a three-dimensional planetary boundary layer scheme," Wind Energy Sci. **7**, 2085–2098 (2022).
[70]B. D. Hirth, J. L. Schroeder, and J. G. Guynes, "Diurnal evolution of wind structure and data availability measured by the DOE prototype radar system," J. Phys. **926**, 012003 (2017).
[71]M. Puccioni *et al.*, "LiDAR measurements to investigate farm-to-farm interactions at the AWAKEN experiment," J. Phys. **2505**, 012045 (2023).
[72]S. B. Roy and J. J. Traiteur, "Impacts of wind farms on surface air temperatures," Proceedings of the National Academy of Sciences of the United States of America **107**, 1045 17899–17904 (2010).
[73]L. Zhou, Y. Tian, S. Baidya Roy, C. Thorncroft, L. F. Bosart, and Y. Hu, "Impacts of wind farms on land surface temperature," Nat. Clim. Change **2**, 539–543 (2012).
[74]C. M. Smith, R. J. Barthelmie, and S. C. Pryor, "*In situ* observations of the influence of a large onshore wind farm on near-surface temperature, turbulence intensity and wind speed profiles," Environ. Res. Lett. **8**, 034006 (2013).
[75]D. A. Rajewski, E. S. Takle, J. K. Lundquist, J. H. Prueger, R. L. Pfeiffer, J. L. Hatfield, K. K. Spoth, and R. K. Doorenbos, "Changes in fluxes of heat, H_2O, and CO_2 caused by a large wind farm," Agric. For. Meteorol. **194**, 175–187 (2014).
[76]S. Wu and C. L. Archer, "Near-ground effects of wind turbines: Observations and physical mechanisms," Mon. Weather Rev. **149**, 879–898 (2021).
[77]M. Calaf, C. Meneveau, and J. Meyers, "Large eddy simulation study of fully developed wind-turbine array boundary layers," Phys. Fluids **22**, 015110 (2010).
[78]M. J. Churchfield, S. Lee, J. Michalakes, and P. J. Moriarty, "A numerical study of the effects of atmospheric and wake turbulence on wind turbine dynamics," J. Turbul. **13**, N14 (2012).
[79]M. L. Aitken, B. Kosović, J. D. Mirocha, and J. K. Lundquist, "Large eddy simulation of wind turbine wake dynamics in the stable boundary layer using the weather research and forecasting model," J. Renewable Sustainable Energy **6**, 033137 (2014).
[80]B. J. Vanderwende, B. Kosović, J. K. Lundquist, and J. D. Mirocha, "Simulating effects of a wind-turbine array using LES and RANS," J. Adv. Model. Earth Syst. **8**, 1376–1390 (2016).

[81]L. P. Chamorro and F. Porté-Agel, "A wind-tunnel investigation of wind-turbine wakes: Boundary-layer turbulence effects," Boundary-Layer Meteorol. **132**, 129–149 (2009).
[82]N. Hamilton, H. Suk Kang, C. Meneveau, and R. Bayoán Cal, "Statistical analysis of kinetic energy entrainment in a model wind turbine array boundary layer," J. Renewable Sustainable Energy **4**, 063105 (2012).
[83]G. V. Iungo, "Experimental characterization of wind turbine wakes: Wind tunnel tests and wind LiDAR measurements," J. Wind Eng. Ind. Aerodyn. **149**, 35–39 (2016).
[84]J. Bartl, F. Mühle, J. Schottler, L. Saetran, J. Peinke, M. Adaramola, and M. Hölling, "Wind tunnel experiments on wind turbine wakes in yaw: Effects of inflow turbulence and shear," Wind Energy Sci. **3**, 329–343 (2018).
[85]S. Kanev, E. Bot, and J. Giles, "Wind farm loads under wake redirection control," Energies **13**, 4088 (2020).
[86]H. Ivanov, S. Dana, and P. Doubrawa, "Loads response that is due to wake steering on a pair of utility-scale wind turbines," Technical Report No. NREL/TP-5000-79187 [National Renewable Energy Laboratory (NREL), Golden, CO, 2021].
[87]S. Dana, H. Ivanov, and P. Doubrawa, "Lifetime fatigue response due to wake steering on a pair of utility-scale wind turbines," J. Phys. **2265**, 022106 (2022).
[88]A. Penã, J. Mann, and N. Dimitrov, "Turbulence characterization from a forward-looking nacelle lidar," Wind Energy Sci. **2**, 133–152 (2017).
[89]S. Letizia, L. Zhan, and G. V. Iungo, "LiSBOA (LiDAR Statistical Barnes Objective Analysis) for optimal design of lidar scans and retrieval of wind statistics—Part 2: Applications to lidar measurements of wind turbine wakes," Atmos. Meas. Tech. **14**, 2095–2113 (2021).
[90]W. Fu, A. Peña, and J. Mann, "Turbulence statistics from three different nacelle lidars," Wind Energy Sci. **7**, 831–848 (2021).
[91]A. Sebastiani, A. Segalini, F. Castellani, and G. Crasto, "Data analysis and simulation of the Lillgrund wind farm," Wind Energy **24**, 634–648 (2020).
[92]G. Centurelli, L. Vollmer, J. Schmidt, M. Dörenkämper, M. Schröder, L. J. Lukassen, and J. Peinke, "Evaluating global blockage engineering parametrizations with LES," J. Phys. **1934**, 012021 (2021).
[93]J. Schneemann, F. Theuer, A. Rott, M. Dörenkämper, and M. Kühn, "Offshore wind farm global blockage measured with scanning lidar," Wind Energy Sci. **6**, 521–538 (2021).
[94]A. Segalini and J. Å. Dahlberg, "Blockage effects in wind farms," Wind Energy **23**, 91–431 (2020).
[95]C. Jacquet, D. Apgar, V. Chauchan, R. Storey, S. Kern, and S. Davoust, "Farm blockage model validation using pre and post construction LiDAR measurements," J. Phys. **2265**, 022009 (2022).
[96]S. Letizia, C. Moss, M. Puccioni, C. Jacquet, D. Apgar, and G. V. Iungo, "Effects of the thrust force induced by wind turbine rotors on the incoming wind field: A wind LiDAR experiment," J. Phys. **2265**, 022033 (2022).
[97]R. K. Newsom, L. K. Berg, W. J. Shaw, and M. L. Fischer, "Turbine-scale wind field measurements using dual-Doppler lidar," Wind Energy **18**, 219–235 (2015).
[98]R. K. Newsom and R. Krishnamurthy, "Doppler lidar (DL) instrument handbook," Technical Report No. DOE/SC-ARM/TR-101 (DOE Office of Science Atmospheric Radiation Measurement (ARM) user facility, 2020).
[99]T. Nishino and R. H. J. Willden, "The efficiency of an array of tidal turbines partially blocking a wide channel," J Fluid Mech. **708**, 596–606 (2012).
[100]T. Nishino and S. Draper, "Local blockage effect for wind turbines," J. Phys. **625**, 012010 (2015).
[101]S. Letizia and G. V. Iungo, "Pseudo-2D RANS: A LiDAR-driven mid-fidelity model for simulations of wind farm flows," J. Renewable Sustainable Energy **14**, 023301 (2022). 10.1063/5.0076739.
[102]S. McTavish, S. Rodrigue, and D. Feszty, "An investigation of in-field blockage effects in closely spaced lateral wind farm configurations," Wind Energy **18**, 1989–2011 (2014).
[103]R. N. King, P. E. Hamlington, K. Dykes, and P. Graf, "Adjoint optimization of wind farm layouts for systems engineering analysis," AIAA Paper No. AIAA 2016-2199, 2016.
[104]J. Å. Dahlberg and D. Medici, "Potential improvement of wind turbine array efficiency by active wake control," in Proceedings of the European Wind Energy Conference Madrid, Spain, 2003.
[105]J. W. Wagenaar, L. Machielse, and J. Schepers, "Controlling wind in ECN's scaled wind farm," in *Proceedings of the European Wind Energy Association (EWEA) Annual Event* (Curran Associates Inc., 2012), pp. 685–694.
[106]S. Boersma, B. M. Doekemeijer, P. M. O. Gebraad, P. A. Fleming, J. Annoni, A. K. Scholbrock, J. A. Frederik, and J. W. V. Wingerden, "A tutorial on control-oriented modeling and control of wind farms," in American Control Conference, 2017.
[107]J. Annoni, C. Bay, K. Johnson, E. Dall'Anese, E. Quon, T. Kemper, and P. Fleming, "Wind direction estimation using SCADA data with consensus-based optimization," Wind Energy Sci. **4**, 355–368 (2019).
[108]M. Sinner, E. Simley, J. King, P. Fleming, and L. Y. Pao, "Power increases using wind direction spatial filtering for wind farm control: Evaluation using FLORIS, modified for dynamic settings," J. Renewable Sustainable Energy **13**, 023310 (2021).
[109]P. Fleming, J. King, E. Simley, J. Roadman, A. Scholbrock, P. Murphy, J. K. Lundquist, P. Moriarty, K. Fleming, J. van Dam, C. Bay, R. Mudafort, D. Jager, J. Skopek, M. Scott, B. Ryan, C. Guernsey, and D. Brake, "Continued results from a field campaign of wake steering applied at a commercial wind farm—Part 2," Wind Energy Sci. **5**, 945–958 (2020).
[110]B. M. Doekemeijer, S. Kern, S. Maturu, S. Kanev, B. Salbert, J. Schreiber, F. Campagnolo, C. L. Bottasso, S. Schuler, F. Wilts, T. Neumann, G. Potenza, F. Calabretta, F. Fioretti, and J.-W. van Wingerden, "Field experiment for open-loop yaw-based wake steering at a commercial onshore wind farm in Italy," Wind Energy Sci. **6**, 159–176 (2021).
[111]E. Simley, P. Fleming, N. Girard, L. Alloin, E. Godefroy, and T. Duc, "Results from a wake-steering experiment at a commercial wind plant: Investigating the wind speed dependence of wake-steering performance," Wind Energy Sci. **6**, 1427–1453 (2021).
[112]M. F. Howland, J. B. Quesada, J. J. P. Martínez, F. P. Larrañaga, N. Yadav, J. S. Chawla, V. Sivaram, and J. O. Dabiri, "Collective wind farm operation based on a predictive model increases utility-scale energy production," Nat. Energy **7**, 818–827 (2022).
[113]J. G. Schepers, T. S. Obdam, and J. Prospathopoulos, "Analysis of wake measurements from the ECN Wind Turbine Test Site Wieringermeer, EWTW," Wind Energy **15**, 575–591 (2012).
[114]L. Vollmer, G. Steinfeld, D. Heinemann, and M. Kühn, "Estimating the wake deflection downstream of a wind turbine in different atmospheric stabilities: An LES study," Wind Energy Sci. **1**, 129–141 (2016).
[115]E. Simley, M. Debnath, and P. Fleming, "Investigating the impact of atmospheric conditions on wake-steering performance at a commercial wind plant," J. Phys. **2265**, 032097 (2022).
[116]D. Bensason, E. Simley, O. Roberts, P. Fleming, M. Debnath, J. King, C. Bay, and R. Mudafort, "Evaluation of the potential for wake steering for U.S. land-based wind power plants," J. Renewable Sustainable Energy **13**, 033303 (2021).
[117]NREL, *FLORIS. Version 3.2.1* (NREL, 2022).
[118]P. A. Fleming, A. P. J. Stanley, C. J. Bay, J. King, E. Simley, B. M. Doekemeijer, and R. Mudafort, "Serial-refine method for fast wake-steering yaw optimization," J. Phys. **2265**, 032109 (2022).
[119]M. Abkar and F. Porté-Agel, "The effect of free-atmosphere stratification on boundary-layer flow and power output from very large wind farms," Energies **6**, 2338–2361 (2013).
[120]J. Meyers and C. Meneveau, "Flow visualization using momentum and energy transport tubes and applications to turbulent flow in wind farms," J. Fluid Mech. **715**, 335–358 (2013).
[121]M. Ge, H. Yang, H. Zhang, and Y. Zuo, "A prediction model for vertical turbulence momentum flux above infinite wind farms," Phys. Fluids **33**, 055108 (2021).
[122]G. Cortina, M. Calaf, and R. B. Cal, "Distribution of mean kinetic energy around an isolated wind turbine and a characteristic wind turbine of a very large wind farm," Phys. Rev. Fluids **1**, 074402 (2016).
[123]A. H. Syed, J. Mann, A. Platis, and J. Bange, "Turbulence structures and entrainment length scales in large offshore wind farms," Wind Energy Sci. **8**, 125–139 (2022).
[124]R. Krishnamurthy, R. K. Newsom, C. M. Kaul, S. Letizia, M. Pekour, N. Hamilton, D. Chand, D. Flynn, N. Bodini, and P. Moriarty, "Observations of wind farm wake recovery at an operating wind farm," Wind Energ. Sci. Discuss. **2024**, 1–37.

[125]R. K. Newsom and R. M. Banta, "Shear-flow instability in the stable nocturnal boundary layer as observed by Doppler lidar during CASES-99," J. Atmos. Sci. **60**, 16–33 (2003).
[126]O. C. Acevedo and D. R. Fitzjarrald, "In the core of the night-effects of intermittent mixing on a horizontally heterogeneous surface," Boundary-Layer Meteorol. **106**, 1–33 (2003).
[127]L. Mahrt, "Intermittency of atmospheric turbulence," J. Atmos. Sci. **46**, 79–95 (1989).
[128]J. Sun, L. Mahrt, R. M. Banta, and Y. L. Pichugina, "Turbulence regimes and turbulence intermittency in the stable boundary layer during CASES-99," J. Atmos. Sci. **69**, 338–351 (2012).
[129]A. Karipot, M. Y. Leclerc, G. Zhang, K. F. Lewin, J. Nagy, G. R. Hendrey, and G. Starr, "Influence of nocturnal low-level jet on turbulence structure and CO_2 flux measurements over a forest canopy," J. Geophys. Res. **113**, D10102, https://doi.org/10.1029/2007JD009149 (2008).
[130]S. Wharton, S. Ma, D. D. Baldocchi, M. Falk, J. F. Newman, J. L. Osuna, and K. Bible, "Influence of regional nighttime atmospheric regimes on canopy turbulence and gradients at a closed and open forest in mountain-valley terrain," Agric. For. Meteorol. **237**, 18–29 (2017).
[131]P. B. S. Lissaman, "Energy effectiveness of arbitrary arrays of wind turbines," J. Energy **3**, 323–328 (1979).
[132]H. Wang, R. J. Barthelmie, S. C. Pryor, and G. Brown, "Lidar arc scan uncertainty reduction through scanning geometry optimization," Atmos. Meas. Tech. **9**, 1653–1669 (2016).
[133]M. L. Aitken and J. K. Lundquist, "Utility-scale wind turbine wake characterization using nacelle-based long-range scanning lidar," J. Atmos. Oceanic Technol. **31**, 1529–1539 (2014).
[134]G. V. Iungo and F. Porté-Agel, "Volumetric lidar scanning of wind turbine wakes under convective and neutral atmospheric stability regimes," J. Atmos. Oceanic Technol. **31**, 2035–2048 (2014).
[135]V. M. Kumer, J. Reuder, B. Svardal, C. Saetre, and P. Eecen, "Characterisation of single wind turbine wakes with static and scanning WINTWEX-W LiDAR data," Energy Procedia **80**, 245–254 (2015).
[136]F. Carbajo Fuertes, C. D. Markfort, and F. Porté-Agel, "Wind turbine wake characterization with nacelle-mounted wind lidars for analytical wake model validation," Remote Sens. **10**, 668 (2018).
[137]L. Zhan, S. Letizia, and G. Valerio Iungo, "LiDAR measurements for an onshore wind farm: Wake variability for different incoming wind speeds and atmospheric stability regimes," Wind Energy **23**, 501–527 (2020).
[138]P. Brugger, C. Markfort, and F. Porté-Agel, "Field measurements of wake meandering at a utility-scale wind turbine with nacelle-mounted Doppler lidars," Wind Energy Sci. **7**, 185–199 (2022).
[139]R. J. Barthelmie and S. C. Pryor, "Automated wind turbine wake characterization in complex terrain," Atmos. Meas. Tech. **12**, 3463–3484 (2019).
[140]J. Gottschall, "Wake measurements with lidar," in *Handbook of Wind Energy Aerodynamics*, edited by B. Stoevesandt, G. Schepers, P. Fuglsang, and S. Yuping (Springer International Publishing, Cham, 2020).
[141]S. Letizia, N. Bodini, P. Brugger, A. Scholbrock, N. Hamilton, F. Porté-Agel, P. Doubrawa, and P. Moriarty, "Holistic scan optimization of nacelle-mounted lidars for inflow and wake characterization at the RAAW and AWAKEN field campaigns," J. Phys. **2505**, 012048 (2023).
[142]S. Letizia, L. Zhan, and G. V. Iungo, "LISBOA (LiDAR Statistical Barnes Objective Analysis) for optimal design of lidar scans and retrieval of wind statistics—Part 1: Theoretical framework," Atmos. Meas. Tech. **14**, 2065–2093 (2021).
[143]R. Vautard, F. Thais, I. Tobin, F.-M. Bréon, J.-G. D. de Lavergne, A. Colette, P. Yiou, and P. M. Ruti, "Regional climate model simulations indicate limited climatic impacts by operational and planned European wind farms," Nat. Commun. **5**, 3196 (2014).
[144]J. M. Tomaszewski and J. K. Lundquist, "Observations and simulations of a wind farm modifying a thunderstorm outflow boundary," Wind Energy Sci. **6**, 1–13 (2021).
[145]F. Letson and S. C. Pryor, "From hydrometeor size distribution measurements to projections of wind turbine blade leading-edge erosion," Energies **16**, 3906 (2023).
[146]K. Panthi and G. V. Iungo, "Quantification of wind turbine energy loss due to leading-edge erosion through infrared-camera imaging, numerical simulations, and assessment against SCADA and meteorological data," Wind Energy **26**, 266–282 (2022).
[147]S. C. Pryor, R. J. Barthelmie, J. Cadence, E. Dellwik, C. B. Hasager, S. T. Kral, J. Reuder, M. Rodgers, and M. Veraart, "Atmospheric drivers of wind turbine blade leading edge erosion: Review and recommendations for future research," Energies **15**, 8553 (2022).
[148]F. Letson, R. J. Barthelmie, and S. C. Pryor, "Radar-derived precipitation climatology for wind turbine blade leading edge erosion," Wind Energy Sci. **5**, 331–347 (2020).
[149]J. I. Bech, C. B. Hasager, and C. Bak, "Extending the life of wind turbine blade leading edges by reducing the tip speed during extreme precipitation events," Wind Energy Sci. **3**, 729–748 (2018).
[150]M. D. Wilkinson, M. Dumontier, I. J. Aalbersberg, G. Appleton, M. Axton, A. Baak, N. Blomberg, J.-W. Boiten, L. B. da Silva Santos, P. E. Bourne, J. Bouwman, A. J. Brookes, T. Clark, M. Crosas, I. Dillo, O. Dumon, S. Edmunds, C. T. Evelo, R. Finkers, A. Gonzalez-Beltran, A. J. G. Gray, P. Groth, C. Goble, J. S. Grethe, J. Heringa, P. A. C. 't Hoen, R. Hooft, T. Kuhn, R. Kok, J. Kok, S. J. Lusher, M. E. Martone, A. Mons, A. L. Packer, B. Persson, P. Rocca-Serra, M. Roos, R. van Schaik, S.-A. Sansone, E. Schultes, T. Sengstag, T. Slater, G. Strawn, M. A. Swertz, M. Thompson, J. van der Lei, E. van Mulligen, J. Velterop, A. Waagmeester, P. Wittenburg, K. Wolstencroft, J. Zhao, and B. Mons, "The FAIR Guiding Principles for scientific data management and stewardship," Sci. Data **3**, 160018 (2016).
[151]M. Macduff and C. Sivaraman, "Preserving data for renewable energy," in AGU Fall Meeting Abstracts, 2017.
[152]P. Moriarty, 2023. "The American WAKE experimeNt (AWAKEN)" Atmosphere to Electrons, U.S. Department of Energy, https://doi.org/10.21947/AWAKEN/1914202.